

CALCAREOUS NANNOFOSSILS AT THE TRIASSIC/JURASSIC BOUNDARY: STRATIGRAPHIC AND PALEOCEANOGRAPHIC CHARACTERIZATION

CINZIA BOTTINI¹, FLAVIO JADOUL¹, MANUEL RIGO^{2,3}, MARIACHIARA ZAFFANI²,
CLAUDIO ARTONI¹ & ELISABETTA ERBA¹

¹*Corresponding author. Department of Earth Sciences, Università degli Studi di Milano, 20133 Milan, Italy. E-mail: cinzia.bottini@unimi.it

²Department of Geosciences, Università degli Studi di Padova, 35131 Padova, Italy.

³IGG - CNR, Via G. Gradenigo 6, 35131 Padova, Italy

To cite this article: Bottini C., Jadoul F., Rigo M., Zaffani M., Artoni C. & Erba E. (2016) - Calcareous nannofossils at the Triassic/Jurassic boundary: stratigraphic and paleoceanographic characterization. *Riv. It. Paleontol. Strat.* 122(3): 141-164.

Keywords: calcareous nannofossils, Triassic/Jurassic boundary, stable isotopes, Lombardy Basin.

Abstract. In this work, calcareous nannofossils are identified for the first time in the uppermost Triassic sequence of the Lombardy Basin (Southern Calcareous Alps, Italy). Two zones are recognized, namely the NT2b (latest Triassic) and the NJT1 (earliest Jurassic). Two species resulted to be good markers to constrain the TJB interval: *Prinsiosphaera triassica* and *Schizosphaerella punctulata*. Nannofossil data are calibrated with C isotopic chemostratigraphy obtained for carbonate and organic matter. Size reduction of *P. triassica* and a decline in the abundance of Triassic nannofossils are detected soon after the “precursor Carbon Isotope Excursion (CIE) and culminated during the “initial negative CIE” characterized by lowest nannofossil abundances and small-sized *P. triassica*. The extinction of Triassic nannofossils occurred in distinctive steps within the “initial negative CIE”, while the Jurassic *S. punctulata* is first observed at the base of the “main negative CIE”. The latest Triassic nannofossil decline in abundance, size reduction and extinctions, represent a progressive deterioration associated to the Central Atlantic Magmatic Province (CAMP) volcanism. Our findings are consistent with nannofossil changes at supraregional scale and indicate that the massive CAMP flood basalts were preceded by initial volcanic pulses. We speculate that a combination of climate change, fertilization and ocean acidification started to influence the calcification process prior to the “initial negative CIE”. Nannoplankton extinctions were not simultaneous and might imply limited capacity for adaptation in the early stages of evolutionary history. However, originations of new taxa soon after the disappearance of Triassic forms suggest the ability to rapidly overcome extreme stressing conditions.

INTRODUCTION

The interval spanning the Triassic/Jurassic boundary (TJB) was marked by a major mass extinction event occurring under profound global environmental changes (e.g., Newell 1963; Raup & Sepkoski 1984; Hallam & Wignall 1997; Olsen et al. 2002; Tanner et al. 2004; McElwain et al. 2009), such as widespread igneous activity in the Central Atlantic Magmatic Province - CAMP (e.g., Marzoli et al. 1999; Schoene et al. 2010; Blackburn et al. 2013), rapid sea-level fluctuations (Hallam & Wignall 1997; Hallam 2002; Guex et al. 2016), and large-scale perturbations of the global carbon cycle (e.g., Ward et al. 2001; Pálffy et al. 2001; Hesselbo et al. 2002; Guex et al. 2004; Ruhl et al. 2010, 2011) also reflected by the collapse of the carbonate biological pump (e.g., McElwain et al. 1999; Hesselbo et al. 2002). The oldest calcareous nannofossils are dated back

to the Late Triassic (Carnian) and their distribution and evolution were described in several works (e.g., Noel 1965; Prins 1969; Di Nocera & Scandone 1977; Moshkovitz 1982; Janofske 1992; Jafar 1983; Bown 1987; Bown 1998; Erba et al. 1992; Bralower et al. 1991, 1992; Bellanca et al. 1993, 1995; Bown et al. 2004; Erba 2006; Onoue & Sano 2007; von Hillebrandt et al. 2007; Clémence et al. 2010). The earliest forms are nannoliths and calcareous dinoflagellates, while coccoliths and non-dinoflagellate nannoliths are found from the Norian. Gardin et al. (2012) provide semi-quantitative estimations of calcareous nannofossil abundances in the Upper Triassic. Since such distributions were constrained by conodont biostratigraphy, they tried to recognize and date the first occurrence of key Upper Triassic nannofossil taxa such as *Prinsiosphaera* and the first “coccolithophores”, which became common in the upper Norian. The Upper Triassic hemipelagic carbonates of southern Italy (Sicanian and Lagonegro Basins) yield relatively abundant nannofossils,

Received: July 27, 2016; accepted: October 25, 2016

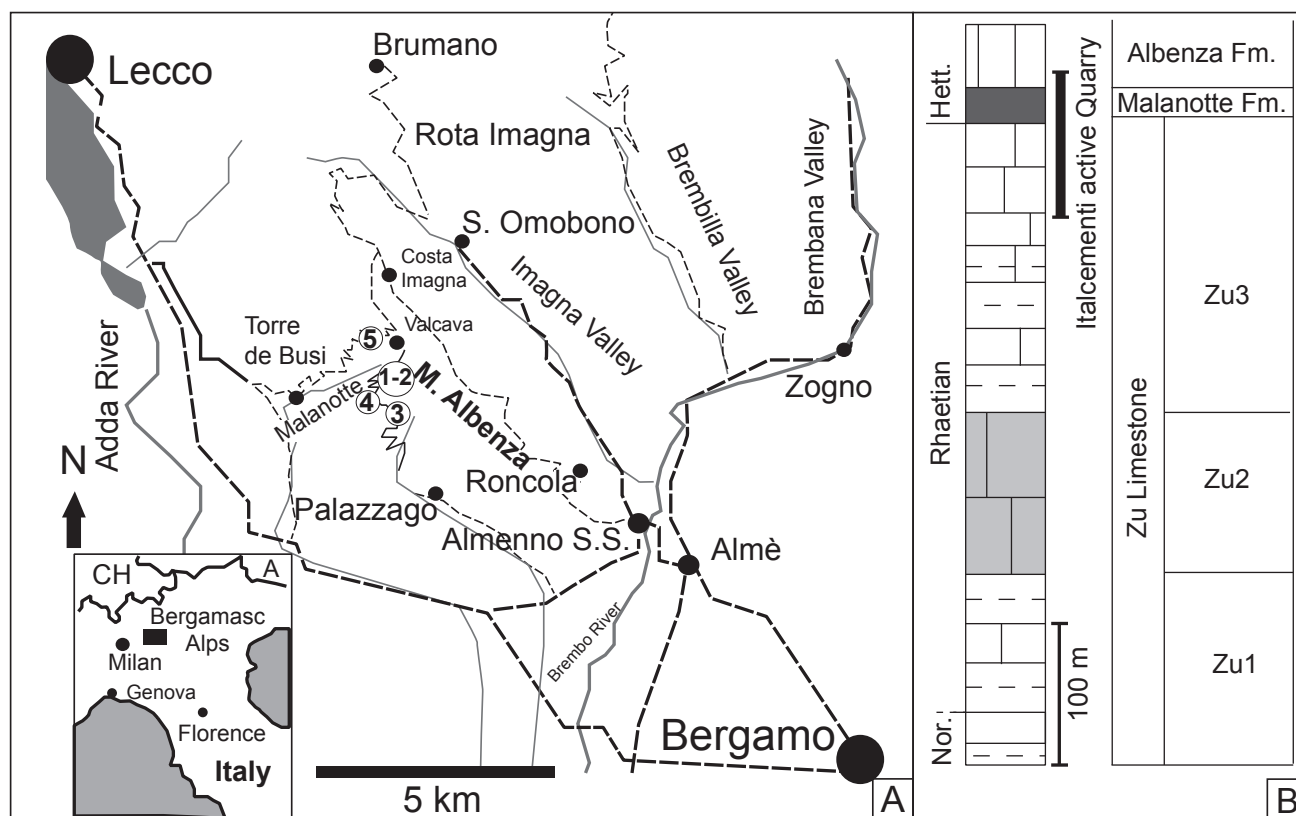


Fig. 1 - A) Location map of the sampling area (modified from Muttoni et al. 2010). Position of: (1) the studied “Italcementi active quarry” section, (2) “Italcementi active quarry” section studied by Bachan et al (2012); (3) “Italcementi inactive quarry section” (Galli et al. 2005 2007), (4) “Malanotte” section (Galli et al. 2005, 2007), (5) “Valcava-Torre de Busi” section (Galli et al. 2007). B) Stratigraphy of the sampled interval, with indication of the stratigraphic interval covered by the studied “Italcementi active quarry” section.

such as calcispheres and nannoliths, suggesting that the early nannoplankton could reach rock-forming abundances even earlier, in the upper Carnian (e.g., Di Nocera & Scandone 1977; Jafar 1983; Janofske 1992; Bellanca et al. 1993, 1995; Preto et al. 2012, 2013a, b). Nevertheless, during the Late Triassic, the pelagic production of carbonate was at its beginning, diversity was very low and the majority of the species did not survive the end-Triassic mass extinction. In fact, it is only from the early Late Jurassic that taxa went through a radiation and progressively became important carbonate producers (Ridgwell & Zeebe 2005), changing the carbonate pelagic productivity (Erba 2006) for the rest of the geological history. Despite the number of manuscripts focusing on Late Triassic nannofossils, little is known about nannofossils around the TJB interval and their recovery during the early Hettangian.

In this work, we investigated the “Italcementi active quarry” section in order to characterize the calcareous nannofossil content across the TJB. The section is located in the Southern Calcareous Alps (Italy), Lombardy Basin, Mt. Albenza (Fig. 1),

and consists of sediments deposited in a shallow subtidal to proximal deep environments, Late Triassic to Early Jurassic in age. Specifically, the TJB is sandwiched between the Rhaetian mainly shallow water inner-middle ramp carbonates of the Zu Limestone Fm. and well bedded, fine grained outer ramp carbonates of the Malanotte Fm., deposited during relative sea-level rise in the latest Rhaetian - earliest Hettangian time interval (e.g., Galli et al. 2005, 2007). Investigation of the nannofossil content was not previously performed in this locality of the Southern Calcareous Alps although nearby sections, as “the Italcementi inactive quarry” and the “Malanotte” sections, were investigated in detail providing a litho-chemo-magneto-biostratigraphy (e.g., Galli et al. 2005, 2007; Jadoul & Galli 2008; Muttoni et al. 2010; Bachan et al. 2012), thus becoming reference-sections for the TJB. The “Italcementi active quarry” section has been specifically selected since it was freshly caved in 2013 and allowed a high resolution sampling across the TJB. It is located very close to the section studied by Bachan et al. (2012) and, together with the “Malanotte” sec-

tion (Galli et al. 2007), is the most complete and expanded section of the Mt. Albenza (Fig. 1) investigated so far. With this study, we intend to increase the existing stratigraphic control on the succession and provide further information for the characterization of the TJB interval, by including nannofossil biostratigraphy and assemblage characterization, as well as new carbon and oxygen stable isotope data.

GEOLOGICAL SETTINGS

In the last decades, several authors have focused on the upper Norian - lower Hettangian succession of the Mt. Albenza since this area, including the “Italcementi quarry” sections, preserves very well exposed outcrops of continuous marine TJB sequence (Lakew 1990; McRoberts 1994; Jadoul et al. 1994, 2004, 2012; Galli et al. 2005, 2007; Jadoul & Galli 2008; Muttoni et al. 2010; Bachan et al. 2012). Specifically, the Norian–Hettangian succession of the Lombardy Basin (Fig. 1) exhibits huge but variable thickness (up to 4.5 Km in the Iseo lake sub-basin), related to different accommodation spaces that have been interpreted to be associated to syndepositional, transtensional tectonic phases. The first tectonic control on the sedimentation started during the Norian (Jadoul et al. 1992) and represents the beginning of the Subalpine passive margin evolution (Bertotti et al. 1993; Jadoul et al. 2004, 2012 and references therein).

In the studied area, the Rhaetian-Hettangian succession is less thick (less than 1000 m), and the depositional system developed on a gently tilted carbonate block (Norian Dolomia Principale/Hauptdolomit) representing the footwall of a narrow N-S oriented structural high, facing a restricted basin named Imagna-Brembilla-Taleggio half graben to the East (Jadoul et al. 1992, 2012). The biostratigraphical and microfacies investigations on the Mt. Albenza succession provided a detailed upper Norian to Hettangian integrated stratigraphy (Galli et al. 2007; Rigo et al. 2009; Muttoni et al. 2010; Jadoul et al. 2012) and allowed to reconstruct the evolution of an articulated carbonate ramp depositional system, characterized by cyclic events of mixed sedimentation and paleogeographic changes. The cyclicity has been interpreted to be periodic and its origin to be mainly related to climatic perturbations, i.e. pluvial events, more persistent during the late Norian (e.g.,

Berra et al. 2010; Trotter et al. 2015), and regional relative sea level changes along a ramp depositional system (3°- 4° order cycles more developed during the Rhaetian) (Lakew 1990; Jadoul et al. 1994, 2012; Galli et al. 2007; Berra et al. 2010). In particular, the shale-marlstone-limestone cyclicity characterizes the upper Riva di Solto Shale and the Zu Limestone fms (uppermost Norian-Rhaetian, Fig. 2), the cycles of which are mainly asymmetrical, 4 to 15 m thick, and dominated by open to restricted subtidal/lagoonal marine low-energy middle outer ramp facies associations, intercalated with high-energy inner ramp carbonates. Marly intercalations are abundant at the base, while the carbonates dominate the top of the cycles and indicate a shallowing upward trend, generally without evidences of exposure surfaces, although thin Fe hardgrounds locally occur at the top of the Zu Limestone Fm. of the Albenza succession (e.g., Zu3 member, Galli et al. 2007). In this context, the TJB is represented by a sharp transition, locally marked by thin Fe hardground (Galli et al. 2007), between the last thick carbonate horizon, rich in megalodontid and shallow water coral (upper Zu3 member, late Rhaetian, Fig. 2), and thin bedded, micritic, poorly fossiliferous limestones of the Malanotte Fm. (Fig. 2). This important boundary correlates across the entire Lombardy Basin and, as indicated also by palynofacies assemblages and chemostratigraphic datasets (Galli et al. 2005, 2007), documents a regional marine transgression, the final crisis of the Rhaetian biogenic carbonate factory and a revolution in the Early Jurassic shallow carbonate factory production and organization (Jadoul & Galli 2008). The overlying 20-30 m thick Malanotte Fm. represents a regional marker useful to identify the TJB on the field throughout the western Southern Alps; only on the Varese structural high this boundary is not preserved, replaced by an unconformity with a “terra rossa” paleosol (Jadoul et al. 2005). The early Hettangian paleogeographic revolution is completed by the overlying bahamian carbonate platform dominated by ooidal bars and peloidal muds, previously known as “Dolomia a Chonchodon” (Gnaccolini 1965; McRoberts 1994) and now named Albenza Formation after Jadoul & Galli (2008).

Lithostratigraphy

The “Italcementi active quarry” section crops out on the Mt. Albenza (45°46'44”N, 9°31'19”E) at

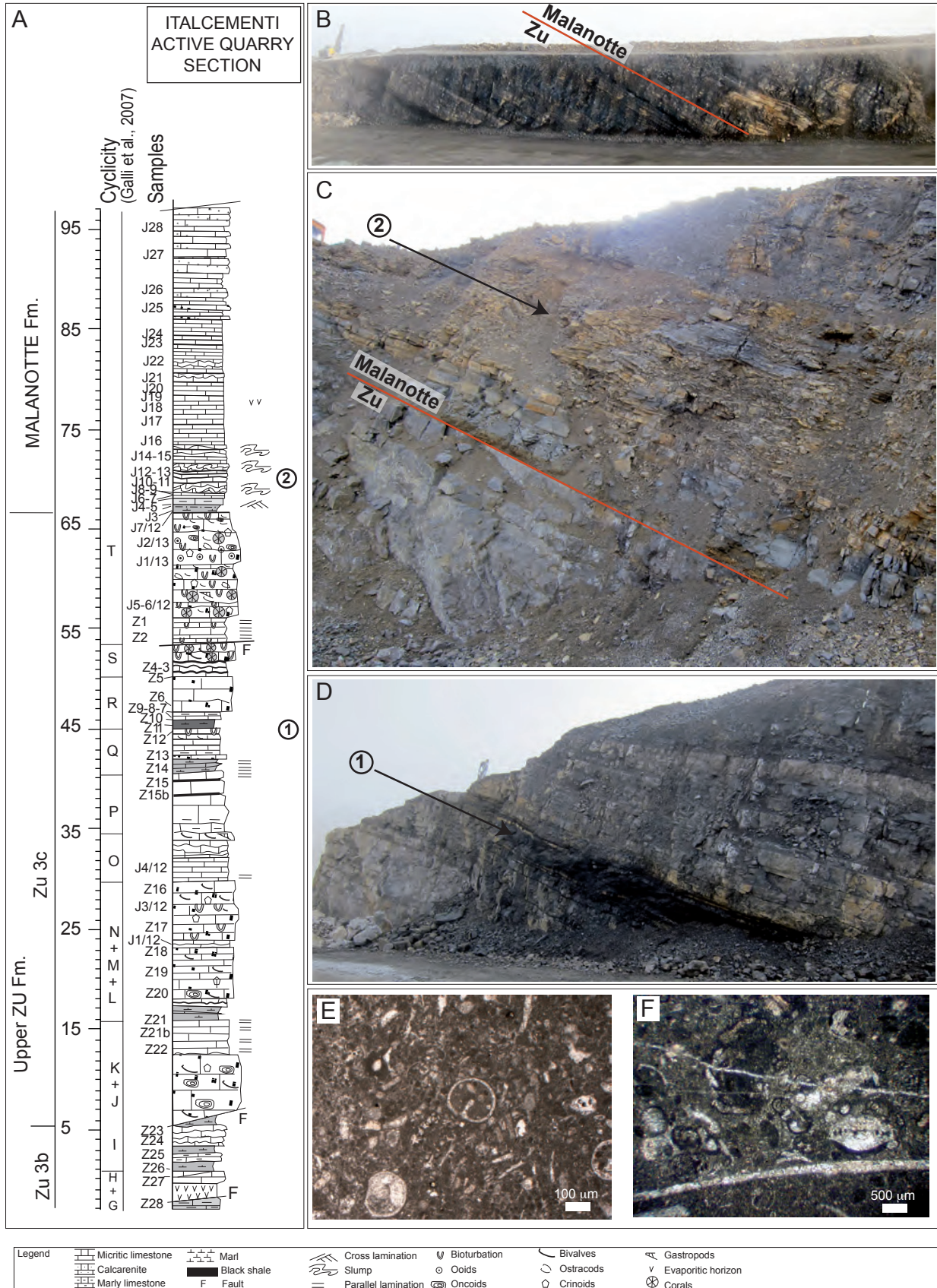


Fig. 2 - A) Lithostratigraphic LOG of the “Italcementi active quarry” section; B) the “Italcementi active quarry” section in 2013 and the position of the Zu Limestone/Malanotte fms boundary; C) detail of the Zu Limestone/Malanotte fms boundary. Slumping in the lower part of the Malanotte Fm are indicated with (2); D) the upper Zu Limestone (Zu3c) characterized by an interval of black shales indicated with (1); E) bioclastic wackestone with gastropodes, and benthic foraminifers (sample J5/12); F) bioclastic wackestone with benthic foraminifers (sample J5/12).

1200 m of altitude and it belongs to the Lombardy Basin (western Southern Alps). The “Italcementi active quarry” section was selected for this work since it was freshly caved in 2013 and allowed a high-resolution sampling across the TJB. The ca. 100 m studied interval (Fig. 2) spans the upper Zu Limestone and the Malanotte fms. The lower-middle portion (69.5 m) corresponds to the top of the Zu Limestone Fm. that includes the Zu3b and Zu3c members (described by Jadoul et al. 1994; Jadoul & Galli 2008), while the overlying 29.5 m correspond to the Malanotte Fm., which is relatively thick and continuous in this section (Fig. 2A, B, C, D).

The Zu lithofacies at the base of the section (Zu3b) is characterized by thin-bedded dark grey lime-mudstones and meter-thick intercalations of marls and marly limestones. A useful lithomarker for regional correlation represented by brownish-yellow vacuolar marly horizons (Galli et al. 2007) occurs at the top of the studied section, close to the boundary with the overlying Zu lithozone (Zu3c). The Zu3c lithozone is mainly calcareous, organized in 5 to 8 m-thick cycles. Marls and marly limestones are abundant in proximity of the lower cycle boundaries. These boundaries, in the studied section, are more transitional respect to the asymmetrical Zu cycles described by Jadoul et al. (1994), Galli et al. (2007), probably because this section represents a basinward portion of the ramp depositional system. Here, the thin Fe-crusts (hardgrounds) characterizing the top cycles of the more proximal ramp successions are missed. A coarsening and shallowing upward trend have been recognized and is represented by a few cycles at the top of the Zu Limestone Fm., which can be easily correlated at local scale. An intercalation of black marls (Fig. 2A, D) is identified at the base of the shallower water, bioclastic pack-grainstone found near the top of the Zu3c. The carbonate microfacies at the cycle base are dominated by fine to coarse peloidal packstone/wackestone with scattered bioclasts (bivalves, echinoids), frequent bioturbation, and small oncoids, associated with laminated lime-mudstone and marly wackestone (Fig. 2A, C, E, F). The microfacies of the middle-upper part of the cycles are more differentiated: the bioturbated intra-bioclastic packstone prevails together with subordinated grainstone rich in oncoid and benthic foraminifera of relatively restricted subtidal environment. The top Zu Limestone microfacies is coarser and shows intercalations of

coral bioclastic grainstone/rudstone of more shallow, inner ramp environment. The sharp boundary with the Malanotte Fm. is in correspondence of a grey marly-silty bed with parallel and also current ripples at the top and scattered small thin mollusc shells. This marker-bed crops out only in the more complete stratigraphic logs of the Albenza area.

The overlying Malanotte Fm. is characterized, at its base, by outer ramp, low energy, not fossiliferous, thin-bedded dark grey lime-mudstone and subordinated peloidal wackestone. Few syndepositional deformations, consisting of few slumping bed markers (Fig. 2A, C), are well recognizable close to the base of this unit and they can be correlated with other slumps recognized in several lower Malanotte sections of the Bergamasc Alps (e.g., Galli et al. 2005, 2007; van de Schootbrugge et al. 2008). The microfacies at the top of the Malanotte Fm. are progressively coarser, characterized by peloidal intraclastic packstone and a few fine-grainstones increasing upwards in abundance.

MATERIAL AND METHODS

Carbon and oxygen isotope analyses

A total of 45 samples were analyzed for $\delta^{13}\text{C}_{\text{carb}}$, $\delta^{18}\text{O}_{\text{carb}}$ and $\delta^{13}\text{C}_{\text{org}}$. For the $\delta^{13}\text{C}_{\text{carb}}$ and $\delta^{18}\text{O}_{\text{carb}}$ measurements, ca. 0.2–0.6 mg of powder were collected in vials and analyzed using a Finnigan Gasbench II connected to a Delta V Advantage mass spectrometer at the University of Padova (Italy). The precision based on replicate analyses of the in-house standard calibrated against NBS-19 (Spotl & Vennemann 2003) is better than $\sigma=0.06\text{‰}$ for $\delta^{13}\text{C}_{\text{carb}}$.

For the $\delta^{13}\text{C}_{\text{org}}$ analyses, ca. 2 g of powder for each sample were dissolved in 25 cl of 3M HCl, for at least 4 hours. The solution was then diluted in 20 cl of deionized water and discarded after centrifuging. The residue was dissolved in 25 cl of 3M HCl in a hot water bath at 70°C for at least 4 hours, and successively neutralized with 20 cl of deionized water and discarded. We repeated the reaction with hot HCl for at least three times per sample, in order to remove possible insoluble carbonate phases (e.g., dolomite, siderite) from the residue. Eventually, the samples were neutralized in deionized water, dried at 40°C overnight, wrapped in tin capsules and analyzed using a Delta V Advantage mass spectrometer connected to a Flash HT Elemental Analyzer at the University of Padova. Multiple blank capsules and isotope standards (IAEA CH-6 = -10.45‰, IAEA CH-7 = -32.15‰, Coplen et al. 2006) were included for each run. The precision, based on replicate analyses of an in-house standard during the period of analyses was better than $\sigma=0.2\text{‰}$ for $\delta^{13}\text{C}_{\text{org}}$.

Calcareous nannofossils

Qualitative and quantitative analyses of calcareous nannofossils were performed on a total of 32 smear slides using standard light microscope techniques under cross polarized and transmitted light, at 1250X magnification. A total of 900 fields of view were studied for each sample, thus covering approximately the entire slide. Smear slides were prepared following the methodology described

by Monechi & Thierstein (1985). A small amount of rock material was powdered into a mortar with few drops of bi-distilled water and posed onto a glass coverslip. Using a toothpick, the suspension was repeatedly smeared along the coverslip until the required thickness of smear was achieved and dried on a hotplate. The coverslip was mounted to the glass slide with Norland Optical Adhesive, and glued by exposure to UV light for a few minutes.

In addition, nannofossils were qualitatively and quantitatively investigated on a total of 16 thin sections polished to an average thickness of 7 μm . Quantitative analyses were performed by counting all specimens in 50 fields of view (corresponding to ca. 1 mm^2). The taxonomic concepts for calcareous nannofossil species identification follow the descriptions by Janofske (1987, 1992), Bown (1987) and Bralower et al. (1991). The adopted nannofossil zonation are after Bralower et al. (1991, 1992) for the Upper Triassic and after Bown (1987) for the Lower Jurassic.

RESULTS

Carbon and oxygen stable isotopes

The carbon isotope data obtained for the “Italcementi active quarry” section show $\delta^{13}\text{C}_{\text{carb}}$ values comprised between -1.95 and 4.48 ‰, while the $\delta^{13}\text{C}_{\text{org}}$ varies between -29.45 and -24.92 ‰ (Appendix I). The measured oxygen isotope values range from -6.86 to -1.12 ‰ (Tab. 1), but they are no further considered in this study since, especially more negative values hint at a possible diagenetic origin and cannot be used as proxy for paleotemperature data. In both $\delta^{13}\text{C}_{\text{carb}}$ and $\delta^{13}\text{C}_{\text{org}}$ profiles, minor and major fluctuations can be noticed. Specifically, from 0 up to 23 m, values are relatively lower (average $\delta^{13}\text{C}_{\text{carb}} = 1.83$ ‰ and $\delta^{13}\text{C}_{\text{org}} = -26.6$ ‰) compared to the average background line (ca. $\delta^{13}\text{C}_{\text{carb}} = 2.5$ ‰, ca. $\delta^{13}\text{C}_{\text{org}} = -26$ ‰). A decrease is then detected between 26 and 58 m. A marked negative shift of ca. 4.5 ‰ in the $\delta^{13}\text{C}_{\text{carb}}$ and ca. 3 ‰ in the $\delta^{13}\text{C}_{\text{org}}$ is recorded between 69.8 and 73.4 m, encompassing the Zu/Malanotte fms transition (Fig. 3). This negative shift is followed by more positive values (average 3.12 ‰ in $\delta^{13}\text{C}_{\text{carb}}$ and -26.9 ‰ in $\delta^{13}\text{C}_{\text{org}}$) up to 81 m, where they start decreasing again down to 1.90 ‰ ($\delta^{13}\text{C}_{\text{carb}}$) and -28.63 ‰ ($\delta^{13}\text{C}_{\text{org}}$).

Calcareous nannofossils

This study revealed the occurrence of calcareous nannofossils and allowed the identification of some species described in literature as well as of other morphotypes that were never described before and/or have not been formalized. All nannofossil specimens are rare throughout the studied interval and their preservation is poor to moderate

with some evidence of overgrowth.

Calcareous nannofossil species are listed in Appendix II. Pictures of the taxa recognized are reported in Plate 1 and include: *Crucirhabdus* sp. cf. *C. minutus*, *Eoconusphaera zambachensis*, *Hayococcus floralis*, *Tetralithus pseudotrifidus*, *Tetralithus cassianus*, *Prinsiosphaera triassica*, and *Schizosphaerella punctulata*. In addition, Plate 2 reports pictures of the unknown morphotypes (named here *Tetralithus* sp., sp. 1, sp. 2, sp. 3, sp. 4 and sp. 5) that are described in Appendix III. A range chart of nannofossils detected in smear slide and thin section is provided in Appendix IV.

Calcareous nannofossil biostratigraph

The identification of nannofossil marker species, their distribution throughout the section as well as the assemblage composition allowed the identification of the NT2b and the NJT1 Zones (Fig. 3): 1) the interval 0 - 71.2 m is characterized by the presence of *Prinsiosphaera triassica*, *Eoconusphaera zambachensis* and *Crucirhabdus* sp. cf. *C. minutus* indicating the uppermost part of the nannofossil Zone NT2b, late Rhaetian in age. This interval is marked also by the presence of other Late Triassic taxa such as *Tetralithus pseudotrifidus*, *Tetralithus cassianus* and *Hayococcus floralis*. These taxa may be diagenetic artefacts, as discussed by Bralower et al. (1991, 1992). In particular, either *T. pseudotrifidus* and *T. cassianus* are interpreted to be inorganic precipitates, whilst *H. floralis* may represent diagenetic replacement of a calcareous nannofossil. Consequently, we include *H. floralis* within the group of nannofossils while *T. pseudotrifidus* and *T. cassianus* are excluded. The interval 73.4 - 98 m is characterized by very low nannofossil abundance and diversity: in fact, only specimens of *S. punctulata* occur, while *P. triassica* and *E. zambachensis* as well as all the other Late Triassic forms are absent. The presence of *S. punctulata* indicates Zone NJT1 of early Hettangian age. The two Zones are separated by a barren interval corresponding to samples at 71.6 m and 72.5 m.

Calcareous nannofossil abundance. The variations of nannofossil abundances are reported in Figure 3 and in the range chart (Appendix IV). The forms recognized are divided into two groups and for each group the total abundance is provided: 1) the nannofossils (nannoliths and coccoliths)

taxonomically defined; 2) the new morphotypes (possible coccoliths and nannoliths) recognized. The nannofossil abundance (identified in smear slide) is generally low throughout the studied interval. Nannofossils are more abundant (average of 11 specimens/900 fields of view) in the lower part of the section (0 - 42 m). A peak up to 21 specimens/900 fields of view is detected at 42 m. From 44.2 m up to 61 m, values are around 6 specimens/900 fields of view. Across the Zu Li limestone/Malanotte transition (69.8 m) a decrease in abundance is detected and two barren samples are encountered (71.6 m - 72.5 m). From the barren interval up to the top of the section, the total abundance stays around 4 specimens/900 fields of view. The interval comprised between 61 m and 69.8 m was not sampled for calcareous nannofossils since it coincides with a coral boundstone. The abundance of the “new morphotypes” shows an average of 10 specimens/900 fields of view in the lower part of the section (0 - 42 m). A peak up to 24 specimens/900 fields of view is detected at 42 m. From 44.2 m up to 60 m, values are relatively lower around 5 specimens/900 fields of view. From 60 m up to 69.8 m the abundance is relatively higher (average of 9 specimens/900 fields of view). At 70 m a decrease in abundance is detected and the samples at 71.6 and 72.5 m are barren. None of the “new morphotypes” is encountered from 73.4 m up to the top of the section.

Prinsiosphaera triassica is found from 0 up to 71.2 m and shows variable size. We distinguished four classes on the basis of the diameter: 1) very large *P. triassica* having a diameter comprised between 10.5 μm and 13 μm , 2) large *P. triassica* having a diameter comprised between 8 μm and 10 μm , 3) medium *P. triassica* having a diameter comprised between 5.5 μm and 7.5 μm and, 4) small *P. triassica* having a diameter < 5 μm . Very large *P. triassica* is found from 0 up to 61 m. The highest abundances are between 0 and 42 m with average of 8 specimens/900 fields of view. From 42 m to 61 m the average abundance of very large *P. triassica* is 2 specimens/900 fields of view. Large *P. triassica* is found from 42 m to 61 m: from 42 m to 48.5 m the average is 3 specimens/900 fields of view and from 49.7 m to 61 m the abundance decreases down to 2 specimens/900 fields of view. Medium *P. triassica* is found from 42 m to 61 m with average abundance of 1 specimens/900 fields of view

between 42 m and 48.5 m and increasing to 2 specimens/900 fields of view between 49.7 m and 61 m. Small *P. triassica* is detected from 69.8 m to 71.2 m and the abundance is comprised between 3 and 4 specimens/900 fields of view. The total abundance of *P. triassica* specimens is higher between 0 and 42 m (average of 8.5 specimens/900 fields of view). A peak in total *P. triassica* abundance is registered at 42 m (14 specimens/900 fields of view) where the very large morphogroup increases in number and the large- and medium-sized specimens first occur. A marked decrease in abundance is detected at 44.2 m and a further decrease is found at 69.8 m. *Crucirhabdus* sp. cf. *C. minutus* is very rare, with abundance of 2-3 specimens/900 fields of view between 0 and 69.8 m. *Eoconusphaera zlambackensis* is also rare from 0 up to 70 m, with abundances around 1-2 specimens/900 fields of view. *Hayococcus floralis* is found at 7.5 m, 28.5 m and 42 m with abundances between 2 and 3 specimens/900 fields of view. *Tetralithus cassianus* is found from 0 to 69.8 m with abundances between 1 and 8 specimens/900 fields of view. Morphotype sp. 1 is found from 0 up to 69.5 m, with abundances comprised between 2 and 8 specimens/900 fields of view. In particular, a peak of 8 specimens/900 fields of view is detected at 42 m. Morphotype sp. 2 is rare and it is found from 34 m up to 70 m with abundances comprised between 2 and 7 specimens/900 fields of view. Morphotype sp. 3 is found from 7.5 m up to 60 m with abundances comprised between 2 and 8 specimens/900 fields of view. Morphotype sp. 4 is detected from 0 up to 70.4 m with abundances comprised between 2 and 4 specimens/900 fields of view. Morphotype sp. 5 is very rare and single specimens have been identified only from 0 up to 45.4 m. *S. punctulata* occurs from 73.4 m up to 98 m with 2-5 specimens/900 fields of view.

The investigation of thin sections indicates the presence of *P. triassica* from 6.2 up to 71.2 m with the highest abundances (8-10 specimens/50 fields of view) in samples at 34 m and 42 m. Morphotype sp. 3 is relatively abundant (2-7 specimens/50 fields of view) from the base of the section up to 70 m. Morphotype sp. 2 is found in samples 42 m, 60 m, 64.9 m and 69.8 m with abundances between 3-7 specimens/50 fields of view. *S. punctulata* is rare (3-5 specimens/50 fields of view) and found at 73.4 m and 90 m.

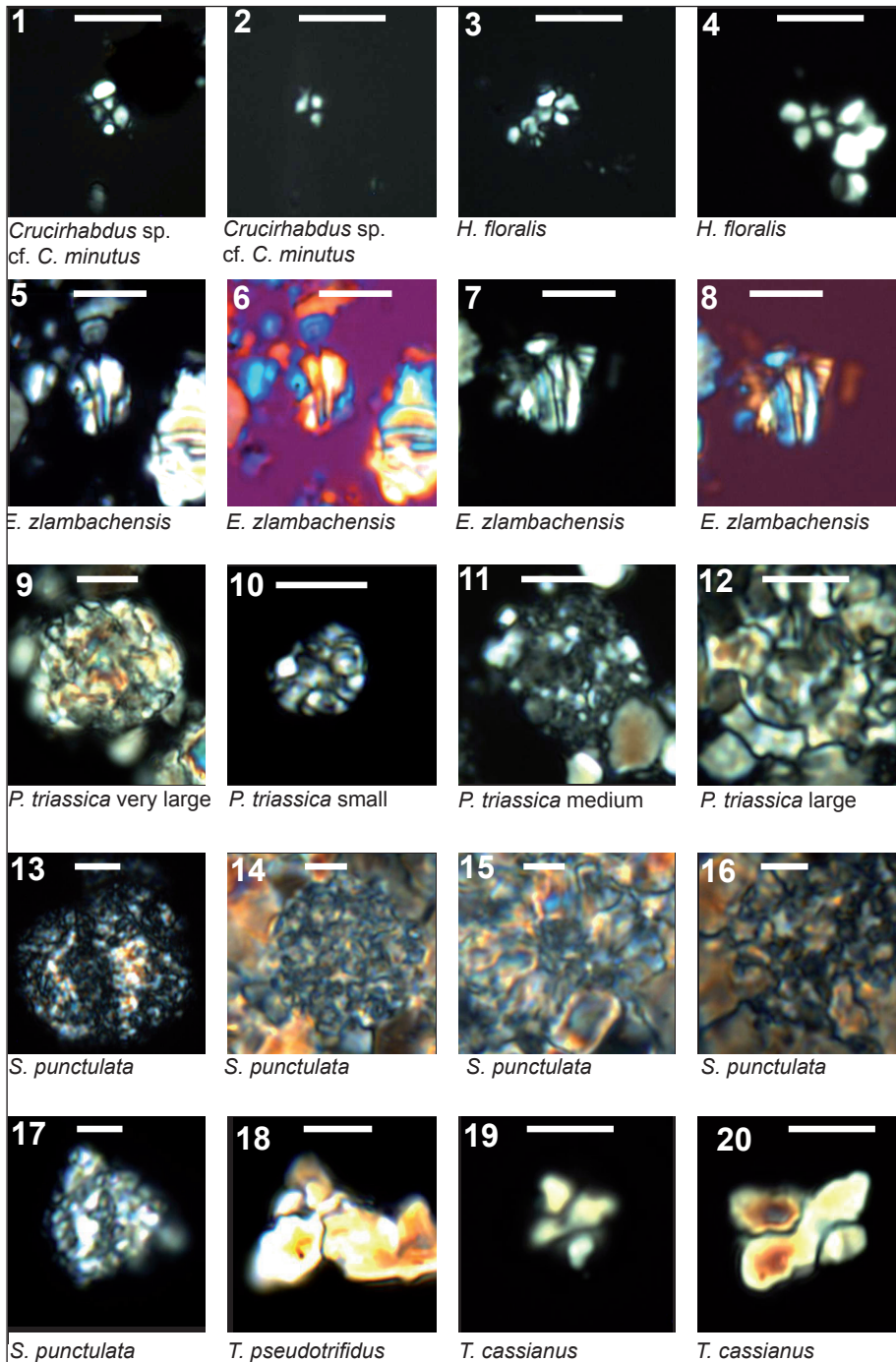


PLATE 1

Calcareous nannofossil under light microscope in smear slides (when not differently specified). Scale bar 5 μm .

- 1) *Crucirhabdus* sp. cf. *C. minutus* (Z17-13);
- 2) *Crucirhabdus* sp. cf. *C. minutus* (J6-12);
- 3) *H. floralis* (Z17-13);
- 4) *H. floralis* (Z25-13);
- 5, 6) *E. zlambachensis* (Z15-13);
- 7, 8) *E. zlambachensis* (J6-12);
- 9) *P. triassica* very large (J4-12);
- 10) *P. triassica* small (J7-12);
- 11) *P. triassica* medium (Z15-13);
- 12) *P. triassica* large (J5-12 m-thin section);
- 13) *S. punctulata* (J25-13);
- 14) *S. punctulata* (J6-13-thin section);
- 15) *S. punctulata* (J25-13-thin section);
- 16) *S. punctulata* (J19-13-thin section);
- 17) *S. punctulata* (J13-13);
- 18) *T. pseudotrifidus* (J7-12);
- 19) *T. cassianus* (Z25-13);
- 20) *T. cassianus* (Z17-13).

DISCUSSIONS

Calcareous nannofossil record in the “Italcementi active quarry” section

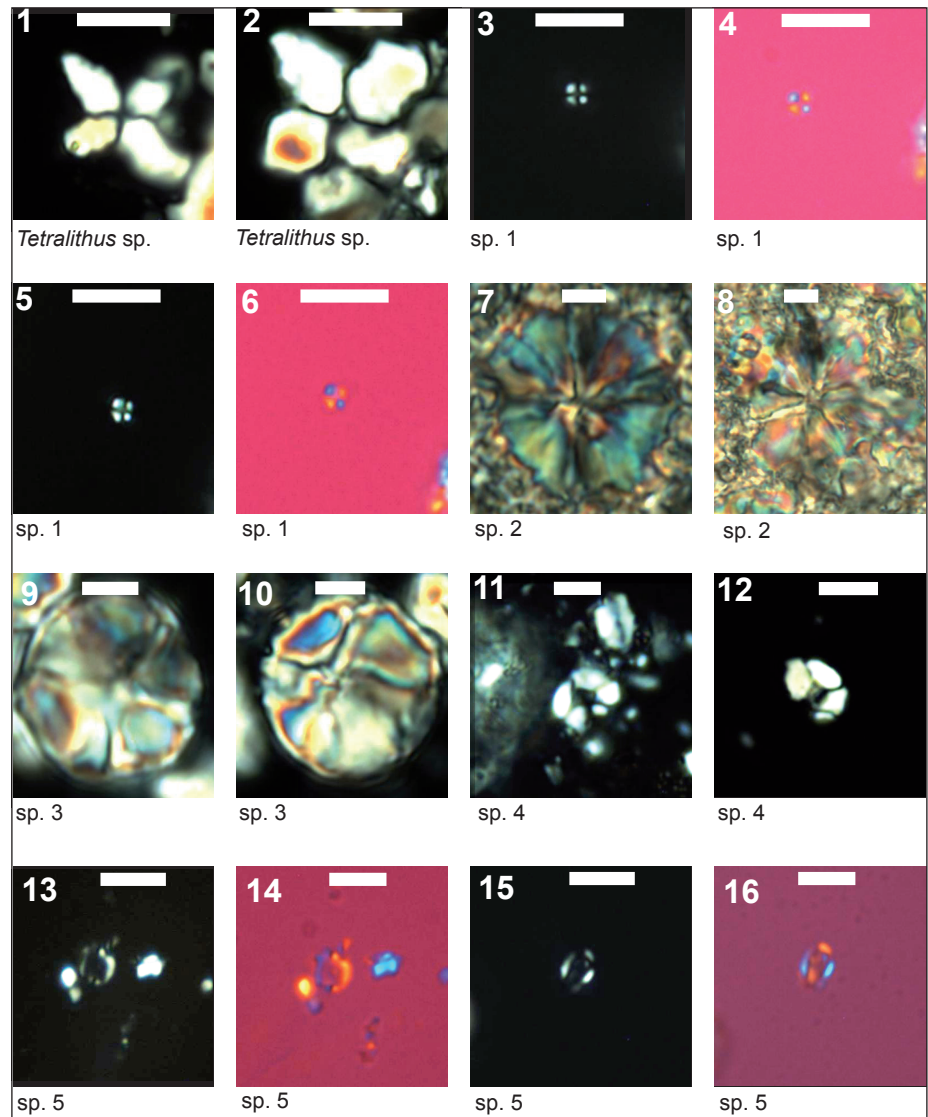
Nannofossil data from literature indicate that the earliest forms of nannoliths and calcispheres made their appearance in the early Carnian and that coccolith species first occurred in the Norian (e.g., Janofske 1990, 1992; Bown 1992; Bralower et al. 1991, 1992; Bellanca et al. 1993; Gardin et al. 2012; Preto et al. 2013a). Over this time interval,

diversity was very low and *Crucirhabdus primulus* (e.g., Bralower et al. 1991, 1992; Bown 1992, 1998) is the only coccolith species known to have survived the end-Triassic extinction. The established zonation scheme for the Upper Triassic (Bralower et al. 1991; Bown 1998) identifies two zones, the NT1 (lower Carnian to lower Norian), and the NT2 divided into two subzones the NT2a (lower to upper Norian) and the NT2b (upper Norian to the TJB). The lower 71.2 m of the “Italcementi active quarry” section correspond to subzone NT2b which is defined

PLATE 2

Nannofossils and “new morphotypes” identified under light microscope in smear slide (when not differently specified). Scale bar 5 μm .

- 1) *Tetralithus* sp. (Z25-13);
- 2) *Tetralithus* sp. (Z15-13);
- 3, 4) sp.1 (Z15-13);
- 5, 6) sp.1 (Z17-13);
- 7) sp. 2 (66.5 m-thin section);
- 8) sp. 2 (66.3 m-thin section);
- 9) sp. 3 (J4-12);
- 10) sp. 3 (Z15-13);
- 11) sp. 4 (Z13-13);
- 12) sp. 4 (Z28-13);
- 13, 14) sp. 5 (Z1-13);
- 15, 16) sp. 5 (J4-12).



by the FO of *E. z̄lambachensis* at the base and by the LO of *P. triassica* at the top. The overlying two samples, 71.6 m and 72.5 m, are barren and from 73.40 m up to the top of the section, the presence of *S. punctulata* indicates Zone NJT1 (Mattioli & Erba 1999).

The nannofossil assemblages found within subzone NT2b, generally compare well with those described from literature in sections spanning the same time interval. Our nannofossil association is, in fact, characterized by the presence of *P. triassica* and *E. z̄lambachensis*, which are identified in several sections worldwide as in NW Australia, (Bralower et al. 1991, 1992), in the British Columbia (Bown 1992) and in the Northern Calcareous Alps (Jafar 1983; Clémence et al. 2010; Gardin et al. 2012) including the Kuhjoch GSSP section (Austria) for the base of the Hettangian (von Hillebrandt et al., 2007). Regarding coccolith species, in the “Italcementi active

quarry” section we detected rare specimens of *Crucirhabdus* sp. cf. *C. minutus* whilst *C. primulus* was not found. The two species are usually found together in the Late Triassic assemblages, as documented by Jafar (1983), Bralower et al. (1991, 1992), and Gardin et al. (2012). Thus, the absence of *C. primulus* in the “Italcementi active quarry” section may be related to poor preservation. Both species are, in fact, dissolution prone and *Crucirhabdus* sp. cf. *C. minutus* is poorly preserved with the cross in the central area not entirely visible. Another coccolith taxon (sp. 5) was identified in few samples (Z28, Z25, Z21b, Z15, Z13) and interpreted to possibly represent poorly preserved specimens of *Archaeozygodiscus keoessensis* (Bown, 1985) and/or corresponding to the “coccolith sp.” reported by Clémence et al. (2010), Preto et al. (2012) and Gardin et al. (2012). We also found specimens of *T. cassianus* and *T. pseudotrifidus* which were encountered in other Norian-Rhaetian

sections (Jafar 1983; Bralower et al. 1991, 1992) but are considered as diagenetic in origin. *Orthopithonella* and *Obliquipithonella* reported by Bralower et al. (1991, 1992), Clémence et al. (2010) and Gardin et al. (2012) in other other Norian-Rhaetian sections were not found in the studied site. At the “Italcementi active quarry” section, the extinction of Triassic nannofossils occurred in three steps (Fig. 3): during step 1 the coccolith *Crucirhabdus* sp. cf. *C. minutus* went extinct, followed by nannoliths *E. z̄lambachensis* (step 2) and small *P. triassica* (step 3). In addition to the taxa mentioned above, our study also highlighted the presence of new morphotypes (sp. 1, sp. 2, sp. 3, sp. 4 and sp. 5) which are present throughout the NT2b subzone and absent in the NJT1 Zone. Their extinction also occurred in three steps at the same stratigraphic levels of the nannofossil extinctions (Fig. 3). During step 1 morphotypes sp. 1 and sp. 3 went extinct followed by morphotype sp. 2 (step 2) and morphotype sp. 4 (step 3). Steps 1 and 2 occurred in two subsequent samples, so we cannot exclude that the extinction level is the same. Our findings indicate that forms sp. 1, sp. 3, sp. 4, and sp. 5 are late Rhaetian in age although we have no data to ascertain their total range. Among these morphotypes, the sp. 2 is probably the same species detected in the Carnian by Bellanca et al. (1995) and Preto et al. (2013a) in Southern Italy, thus indicating that this taxon had a relatively long range extending from the Carnian up to the end of the Rhaetian. The presence of the short barren interval (samples 71.6 m and 72.5 m) in the TJB interval, does not allow to exclude that some/all of the Triassic nannofossil species identified, coexisted with *S. punctulata* which has its FO right above the barren interval. At Kuhjoch section, very rare specimens of *P. triassica* and *E. z̄lambachensis* are found together with calcispheres and *S. punctulata* above the TJB, although the authors stated that the two species are probably reworked (von Hillebrandt et al. 2007). We also notice that, similarly to the “Italcementi active quarry” section, at Kuhjoch section the LO of *E. z̄lambachensis* preceded the LO of *P. triassica*. Clémence et al. (2010) described the presence of “schizosphaerellids” (specimens with shape and optical properties almost identical to the Jurassic genus *Schizosphaerella*) in the uppermost Rhaetian in assemblages containing *P. triassica*. They also found “schizosphaerellids” in the lowermost Hettangian, although *S. punctulata* is never reported

throughout the sections.

At St. Audrie’s Bay section (UK), *S. punctulata* was found together with *C. primulus* (van de Schootbrugge et al. 2007), at a lower level with respect to the FO of the ammonite *Psiloceras planorbis*.

If we take under consideration the studies presenting nannofossil biostratigraphic data across the TJB as well as our new dataset, the two nannofossil events which are good markers in the TJB interval are the LO of *P. triassica* and the FO of *S. punctulata*: they are dissolution resistant species and are found in all records. In particular *P. triassica* is always the last nannofossil species to go extinct. The other taxa, as *E. z̄lambachensis*, *C. minutus*, *C. primulus*, *A. koessensis* are more easily affected by diagenesis and/or are very rare. The data collected confirm previous observations suggesting that the TJB interval is marked by a major change in the assemblage composition and in diversity. The identification of new morphotypes in the Rhaetian (this study) implements the characterization of the Late Triassic assemblages and the TJB boundary interval.

Stratigraphic characterization of the TJB interval in the Southern Calcareous Alps

The late Rhaetian-early Hettangian succession of the Mt. Albenza (Lombardy Basin) was extensively investigated in the last decades and integrated stratigraphy is available for several sections located in the Lombardy Basin (e.g., Lakew 1990; McRoberts 1994; Jadoul et al. 1994, 2004, 2012; Galli et al. 2005, 2007; Jadoul & Galli 2008; Muttoni et al. 2010; Bachan et al. 2012; van de Schootbrugge et al. 2008). The succession preserves very well exposed outcrops of mostly continuous and expanded marine TJB sequence and, therefore, constitutes the reference for this interval in the Southern Calcareous Alps. In order to provide a comprehensive stratigraphic characterization of the studied site, we correlated our studied section (Fig. 6) with three nearby (hundreds of meters) successions namely the “Italcementi active quarry” section (studied by Bachan et al. 2012), the “Italcementi inactive quarry” and the Malanotte sections (studied by Galli et al. 2005; 2007; Muttoni et al. 2010), and the Adrara section (from Galli et al. 2005, 2007; van de Schootbrugge et al. 2008) that is situated in the eastern Bergamasca Alps. The correlation is based on lithostratigraphy and, specifically, we identified within the Zu3c, the Malanotte and the overlying Albenza fms, a total of

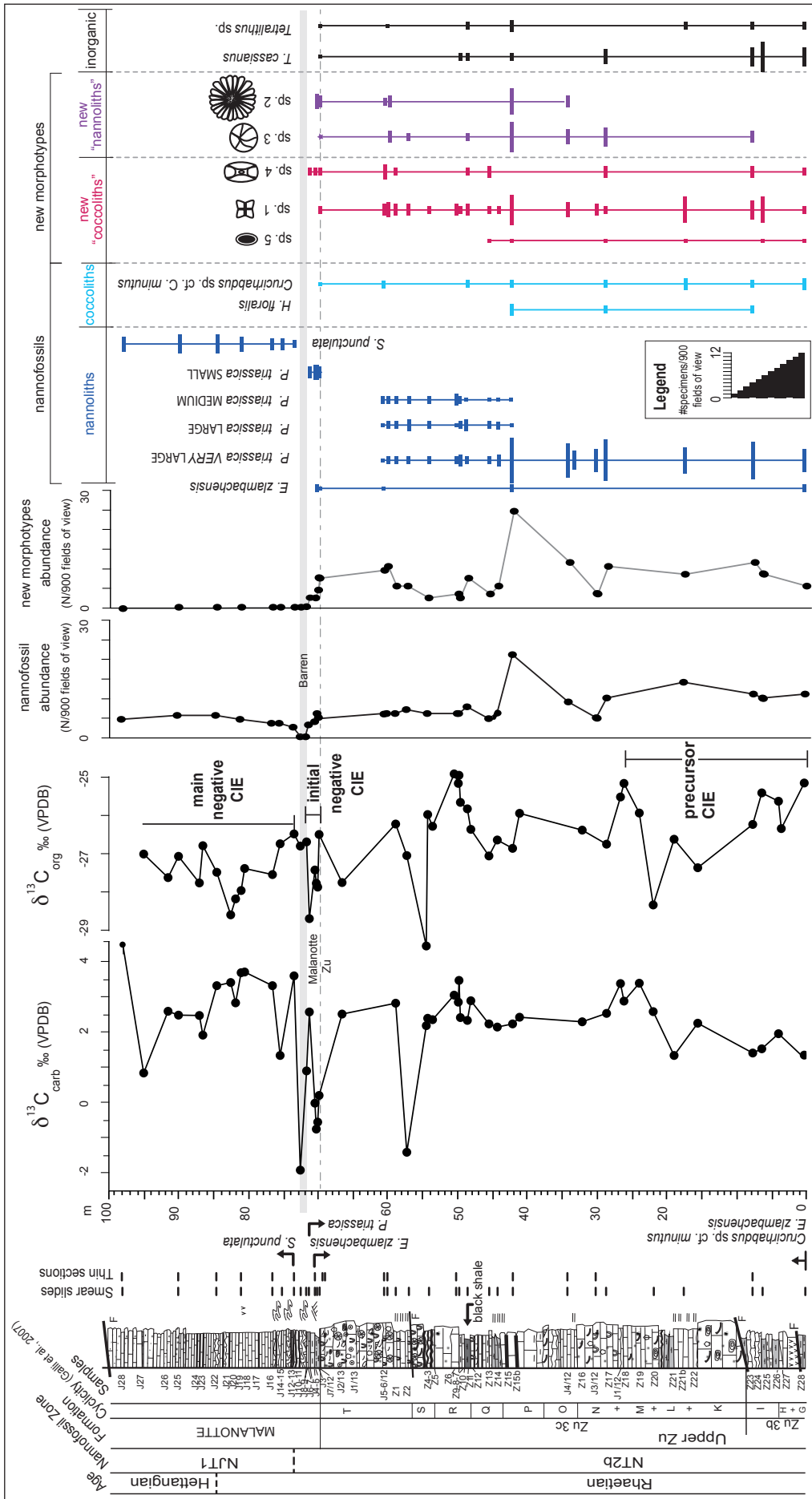


Fig. 3 - Calcareous nannofossil events (First and Last Occurrences, FO and LO respectively), Zones and abundance variations identified in the “Italcementi active quarry” section plotted against chemostratigraphy. The nanofossil total abundance and the “new morphotypes” total abundance in smear slides are expressed as the total number of specimens found in 900 fields of view. Single taxon and “new morphotype” abundances are indicated. Very large *P. triassica* 10.5 $\mu\text{m} < \text{O} < 13 \mu\text{m}$, large *P. triassica* 8 $\mu\text{m} < \text{O} < 10 \mu\text{m}$, medium *P. triassica* 5.5 $\mu\text{m} < \text{O} < 7.5 \mu\text{m}$, small *P. triassica* $\text{O} < 5 \mu\text{m}$. The TJB is placed according to the GSSP definition. The lithological legend is reported in Fig. 2.

7 intervals corresponding to lithofacies showing similar lithological features listed as follow (Fig. 6):

Interval A) includes the Zu3c up to the base of the coral boundstone which characterizes the uppermost part of the Zu3c. The Zu3c consists of mainly laminated calcareous mudstones with thin shale intercalations. Within this interval a black shale layer is detected and is considered as a regional marker bed.

Interval B) coincides with the coral boundstone layer at the very top of the Zu3c being characterized by very rich fossil assemblages (benthic foraminifers, corals, calcisponges, bryozoans, with large megalodontids and oncoidal limestone).

Interval C) consists of ca. 1-2 meters-thick marly silty horizon at the base of the Malanotte Fm. where the rich and diversified fauna disappears.

Interval D) is represented by an interval of slumped thin-bedded mudstones with shale intercalations.

Interval E) coincides with grey calcareous mudstones and marly layers.

Interval F) is marked by increase in calcarenite beds consisting of bioclastic wackestones-packstones.

Interval G) is represented by a thin bedded dark grey fine oolitic grainstones at the base of the Albenza Fm. In the considered sections, most of these intervals are present and show comparable thicknesses. However, the lower part of the Zu3c was not studied (Galli et al. 2005, 2007) in the “Italcementi inactive quarry” and the Malanotte sections, thus there is no record available for this interval. In the “Italcementi inactive quarry” section the transition between the Zu3c and the Malanotte Fm. is marked by a thin Fe hardground and the marly layer is not present probably elided by a hiatus (Galli et al. 2007). In our studied site a fault marks the top of the Malanotte Fm. and the overlying Albenza Fm. was not sampled. In the Adrara section a few intervals were not recovered in the Zu3c and a gap of ca. 8 m occurs within the calcareous mudstones and wackestones of the Malanotte Fm. (Galli et al. 2005, 2007; van de Schootbrugge et al. 2008).

In the studied site, the new nannofossil data indicate the presence of Triassic nannofossil species in the Zu Limestone Fm. (Zu3c) and in the lowermost part (ca. 1.5 m) of the Malanotte Fm., within the marly horizon (Interval C), where they go extinct. The extinction of the Triassic nanno-

fossils corresponds to a negative shift of ca. 4‰ in both the organic and inorganic carbon isotope records. The FO of the Jurassic species *S. punctulata*, accompanied by a change in the nannofossil assemblage, occurs at ca. 3.6 m above the Zu Limestone/Malanotte fms boundary, above the $\delta^{13}\text{C}$ negative anomaly and at the base of the calcareous mudstones (Interval E).

Galli et al. (2005, 2007) identified the LO of *Rhaetipollis germanicus* within the marly horizon in the lowermost part of the Malanotte Fm. (Interval C). In the “Italcementi inactive quarry”, Malanotte and Adrara sections (Fig. 6), the FO of *Krauselisporites reissingeri*, associated with other diagnostic Hettangian pollens as *C. macroverrucosus*, occurs within the calcareous mudstones of the Malanotte Fm. (Interval E) and shows the highest abundances up to the base of the calcarenites. The dataset of Galli (2002), Galli et al. (2005, 2007) shows that these events occur at equivalent lithostratigraphic levels in other sections of the Lombardy Basin. Magnetostratigraphy, available for the “Italcementi inactive quarry” section, shows a reversal, interpreted to correspond to the E23r, occurring within the coral boundstone layer (Interval B) at the topmost part of the Zu3c (Muttoni et al. 2010).

For most sections of the Lombardy Basin, C-isotope data of bulk carbonate are available, whilst only a few sections were also characterized for $\delta^{13}\text{C}_{\text{org}}$, as for example the “Italcementi inactive quarry” and Adrara sections (Galli et al. 2005, 2007; van de Schootbrugge et al. 2008) (Fig. 4). In our studied site, the $\delta^{13}\text{C}_{\text{carb}}$ and $\delta^{13}\text{C}_{\text{org}}$ profiles show larger and minor fluctuations, but only five “negative” anomalies are detected in both $\delta^{13}\text{C}_{\text{carb}}$ and $\delta^{13}\text{C}_{\text{org}}$ profiles and are listed as follows (the numbering is also reported in Fig. 4):

- 1) an interval of isotopic values being ca. 2 to 3 ‰ lower than background values in the lower part of the Zu3c Fm.;
- 2) a ca. 5 m-thick interval of the Zu3c, in correspondence of marl layers, showing a minor shift towards ca. 1 ‰ lower $\delta^{13}\text{C}$ values;
- 3) a short-lived negative spike characterizing the middle part of the Zu3c Fm., although the lowest values are given by two datapoints (one for the $\delta^{13}\text{C}_{\text{carb}}$ and one for the $\delta^{13}\text{C}_{\text{org}}$) spaced a few centimetres one from another;
- 4) a negative spike marking the marly layer at the base of the Malanotte Fm. The negati-

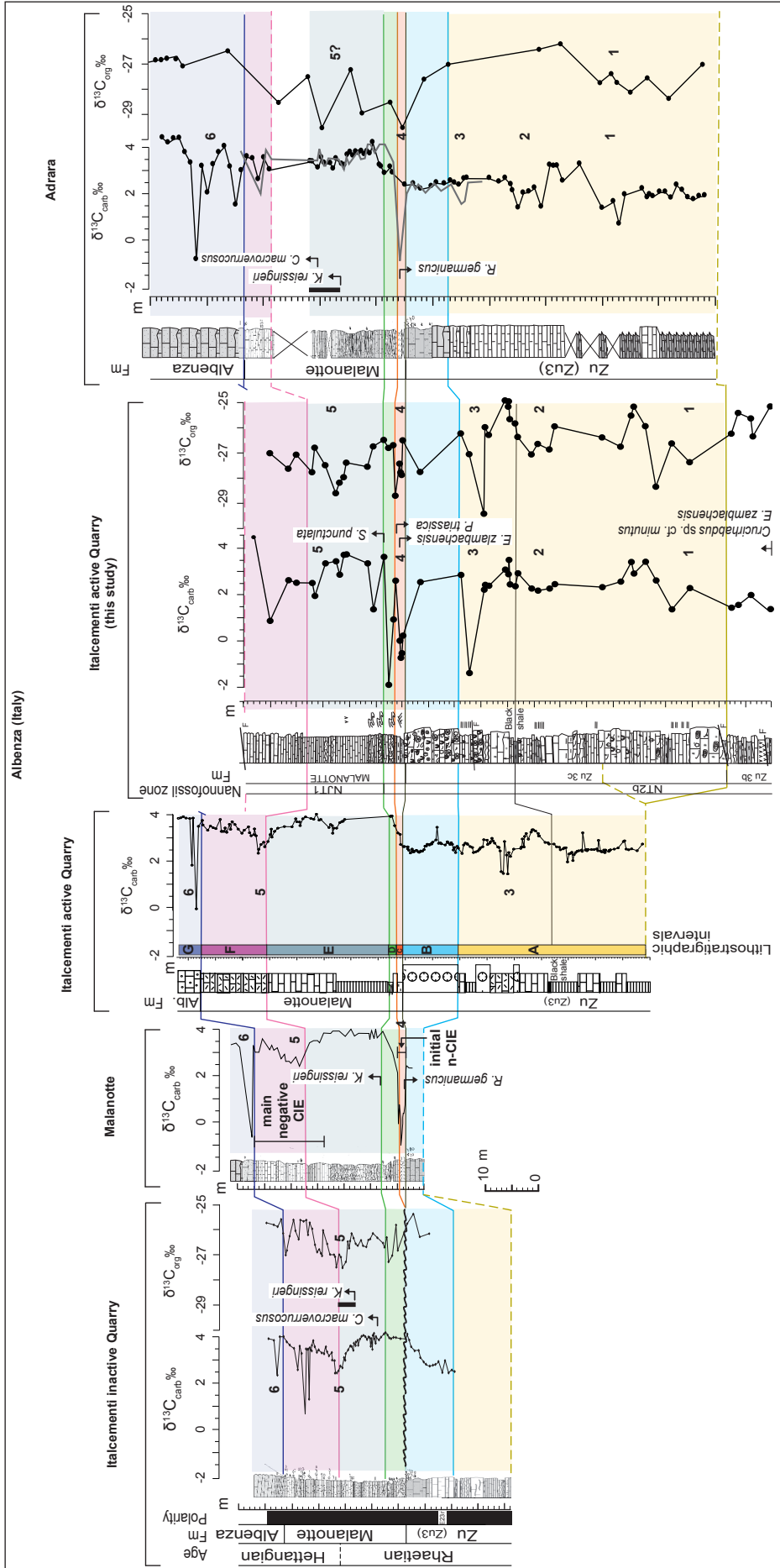


Fig. 4 - Correlation between the “Italcementi active quarry” section and published data for the Lombardy Basin (Italy). The sections presented are: the “Italcementi inactive quarry” and the “Malanotte” sections studied by Galli et al. (2005, 2007) and Muttoni et al. (2010), the “Italcementi active quarry” section studied by Bachan et al. (2012); the Adrara section studied by Galli et al. (2005, 2007) and van de Schootbrugge et al. (2008). Numbers 1 to 6 identify the sequence of C-isotope anomalies identified in this work. The correlation is based on lithostratigraphy and 7 intervals, labelled A to G, are highlighted: A) includes the Zu3c up to the base of the coral boundstone; B) coincides with the coral boundstone layer; C) consists of ca. 1-2 meters-thick marly silty horizon; D) is an interval of slumped thin-bedded mudstones; E) coincides with grey calcareous mudstones and marly layers; F) consists of calcarenites; G) is a thin bedded dark grey fine oolitic grainstones. Legend of symbols for the “Italcementi active quarry” section is reported in Fig. 2. The lithological logs of the other sections are taken from literature.

ve shift is followed by higher values being around the background line for the $\delta^{13}\text{C}_{\text{org}}$ and above the background line for the $\delta^{13}\text{C}_{\text{carb}}$. The positive $\delta^{13}\text{C}_{\text{carb}}$ interval is interrupted by two further negative values;

5) a longer interval (ca. 20–25 m) of relatively lower isotopic values in the middle-upper part of the Malanotte Fm.

Some of these five anomalies can also be detected in the C-isotope profiles of the other considered sections and are therefore labelled with the same sequence of numbers (Fig. 4). The similarities in the C-isotope records suggest a primary isotopic signal. In the Adrara section (Galli et al. 2005, 2007; van de Schootbrugge et al. 2008) the record shows three excursions towards lower C-isotopic values within the Zu3c (1, 2 and 3; Fig. 4) but the second and third ones are recorded only in the $\delta^{13}\text{C}_{\text{carb}}$. One negative spike (4) is present at the base of the Malanotte Fm. The record through the Malanotte Fm. (Interval E) is not complete and only the $\delta^{13}\text{C}_{\text{org}}$ shows relatively lower values (5?). Within the Albenza Fm., the $\delta^{13}\text{C}_{\text{carb}}$ is scattered down to very negative values (6) (not recorded in the $\delta^{13}\text{C}_{\text{org}}$). In the “Italcementi active quarry” section (Bachan et al. 2012), a relative decrease in $\delta^{13}\text{C}_{\text{carb}}$ values is shown in the middle of the Zu3c (3) just above the black shale interval. Another anomaly towards lower values (5) is detected in the middle of the Malanotte Fm. (Interval E), and very negative spikes are recorded in the Albenza Fm. (6). In the Malanotte section (Galli et al. 2005; 2007) a marked negative interval characterizes the marly layer at the base of the Malanotte Fm. (4); an interval of lower C-isotope values is detected in the middle-upper part of the Malanotte Fm. (5), and a negative spike marks the lowermost part of the Albenza Fm. (6). In the middle-upper part of the Malanotte Fm. of the “Italcementi inactive quarry” section, a negative interval is recorded (5), followed by a negative spike (6) occurring at the base of the Albenza Fm. (Galli et al. 2005; 2007). Galli et al. (2005; 2007) interpreted the absence of the negative shift in the “Italcementi inactive quarry” section at the base of the Malanotte Fm. as due to a hiatus eliding the marly layer at the base of the Malanotte. In these sections, the transition between the Zu3c and the Malanotte Fm. is marked by thin Fe hardground. Instead, in the “Italcementi active quarry” section studied by Bachan et al. (2012), the absence of the negative

spike is probably due to low sampling resolution over this interval related to poor exposure (as also stated by the authors). The negative anomaly is, in fact, very short-lived and it is recorded in a few decimetres in the core of the marly layer of the Malanotte Fm. It is therefore plausible that Bachan et al. (2012) sampled only the base and top of the marly layer thus missing the negative shift.

The correlation and integration of the stratigraphic information available for the sections presented in Fig. 4, shows that the late Rhaetian Zu3c was characterized by the occurrence of Triassic pollen and nannofossils and was marked by at least three anomalies in the C-isotope record that were never identified and/or correlated in previous works. The base of the Malanotte Fm. clearly marks a major change in the environmental conditions and consequently in the biotic communities (as extensively discussed by Galli et al. 2005; 2007). This interval is marked by the extinction of either nannofossil and pollen Triassic forms as well as of the rich and diversified benthic foraminiferal assemblages and reef-associated organisms. It is marked also by a negative C-isotope anomaly (4), interpreted by different authors (e.g., Galli et al. 2005, 2007; Bachan et al. 2002; Schootbrugge et al. 2008; Felber et al. 2015) as possibly corresponding to the conventionally called “initial negative Carbon Isotope Excursion (CIE)” (Hesselbo et al. 2002; Ruhl et al. 2009). This anomaly is found in most of the Mt. Albenza sections, except where a hiatus elides the base of the Malanotte Fm., being anyhow indicator of a possible major perturbation in the basin system. The appearance of the palynomorphs and nannofossils accompanied by a progressive recovery of marine ecosystems, coincides with the onset-early phase of the subsequent longer anomaly in the C-isotope interpreted as the equivalent of the “main negative CIE” (e.g., Galli et al. 2005; 2007; Bachan et al. 2002; Schootbrugge et al. 2007, 2008). In the studied “Italcementi active quarry” section the uppermost part of the anomaly was not sampled.

Correlation with records from the Northern Calcareous Alps and England

A large amount of data is available on sections worldwide spanning the TJB interval. Here, we consider two of the most complete and stratigraphically constrained sections for comparison with the data from the Mt. Albenza succession: the Kuhjoch

GSSP section (Northern Calcareous Alps, Austria) for the base of the Hettangian and St. Audrie's Bay section (UK). Three main "negative" $\delta^{13}\text{C}$ anomalies were identified across the TJB interval and are conventionally named as follows: 1) the "precursor CIE", traced in the lower Rhaetian at St. Audrie's Bay (Ruhl & Kürschner 2011) and identified in other sites (e.g., Austria, Germany, Ruhl and Kürschner 2011); 2) the "initial negative CIE", being short-lived and of relatively high amplitude (ca. 5 ‰ in the $\delta^{13}\text{C}_{\text{org}}$), recognized at Kuhjoch, St. Audrie's Bay and in sections worldwide (e.g., Austria, McRoberts et al. 1997; Ruhl et al. 2011; Felber et al. 2015; Queen Charlotte Island, Canada, Ward et al. 2001; 2004, Whiteside & Ward 2011; Hungary, Pálffy et al. 2001, southwest England, Hesselbo et al. 2002; Ruhl et al. 2010; Nevada, Guex et al. 2003, 2004; Italy, van de Schootbrugge et al. 2008; Bachan et al. 2012); 3) the "main negative CIE", which has a longer extent and it is detected not only at Kuhjoch and St. Audrie's Bay but also in many sections worldwide (e.g., van de Schootbrugge et al. 2008; Ruhl et al. 2010, 2011; Bachan et al. 2012; Felber et al. 2015).

The base of the Hettangian is formally placed at the FO of the ammonite *Psiloceras spelae* that, at the GSSP Kuhjoch section (Austria), occurs ca. 6 m above the "initial negative CIE", in the core of the "main negative CIE" (von Hillebrandt et al. 2007). The extinction of the Triassic forms (e.g., calcareous nannofossils, palynomorphs, ammonoids) at the GSSP section as well as in other sections coincides with the "initial negative CIE", whilst the level of the FO of Jurassic species differs among sites and fossil groups. At Kuhjoch section, the FO of the nannofossil *S. punctulata* occurs at the onset of the "main negative CIE" (von Hillebrandt et al. 2007) below the FO of the Jurassic pollen *C. thiergartii* and ammonoid *P. spelae*. The base of the acme of the pollen *K. reissingeri* coincides with the FO of *P. spelae*. At St. Audrie's Bay section, the FO of *S. punctulata* occurs together with *C. thiergartii* (van de Schootbrugge et al. 2007), at a lower level with respect to the FO of the ammonite *Psiloceras planorbis* (Ruhl et al. 2009; Bonis et al. 2010) at the base of the "main negative CIE". The FO of *K. reissingeri* is found slightly below the FO of *C. thiergartii*.

On the basis of chemostratigraphy, and in particular of the organic C-isotope record which displays clearer fluctuations, we propose and discuss a possible correlation of the studied site (and

the record of the Mt. Albenza) with Kuhjoch and St. Audrie's Bay sections. The C-isotope anomaly at the base of the Zu3c is identified as the "precursor CIE" (Fig. 5). The absence of a record below this interval for the studied site does not allow to unambiguously identify the negative anomaly as the "precursor CIE" and/or exclude that it is entirely recorded. Nevertheless, it is consistent with the age assignment based on nannofossils and the absolute values of the organic C-isotope record. If this interpretation is correct, it would be the first evidence in the Mt. Albenza succession of the "precursor CIE". The anomalies in the middle part of the Zu3c may eventually correlate with the minor shifts occurring between the "precursor CIE" and the "initial negative CIE". The C-isotope shift at the base of the Malanotte Fm. is here interpreted to be the equivalent of the "initial negative CIE", and the longer interval of lower C-isotope values in the middle-upper part of the Malanotte Fm. to be the "main negative CIE" although probably not complete, since the uppermost part is missing. This interpretation is mostly in agreement with the interpretation of Galli et al. (2005, 2007), van de Schootbrugge et al. (2008); Bachan et al. (2012) on the basis of datasets from other sections of the Lombardy Basin. The interpretation of the isotope profiles is also in agreement with the position of the magnetic reversal E23r (Muttoni et al. 2010), which would occur just below the "initial negative CIE". However, this chemostratigraphic interpretation largely differs from what reported by Felber et al. (2015), who interpret the isotopic values within the Malanotte Fm. from the end of the "initial negative CIE" up to the base of the Albenza Fm. as corresponding to the positive interlude preceding the "main negative CIE".

The position of the nannofossil and pollen bioevents with respect to the "initial negative CIE" is similar to that of the bioevents of the same fossil groups detected in the two reference sections: the extinction of the Triassic forms occurs at the same stratigraphic level in all sections and coincides with the "initial negative CIE". The interval of higher C-isotope values, which separates the "initial negative CIE" from the "main negative CIE", is instead shorter in the "Albenza sections" compared to Kuhjoch and St. Audrie's Bay sections. It is plausible that the interval of higher C-isotope values is somehow condensed and perhaps partially missing in the "Italcementi active quarry" section. However,

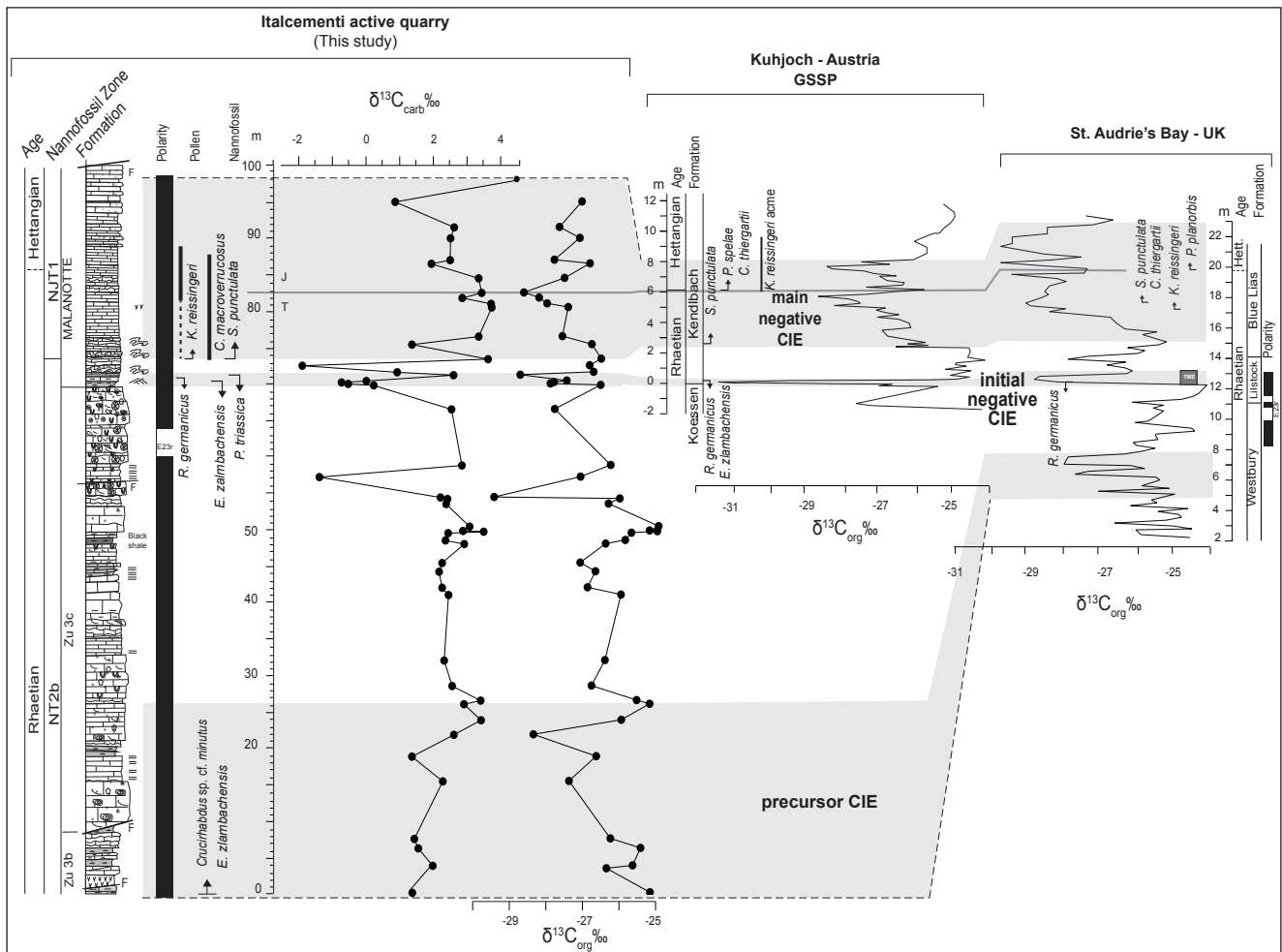


Fig. 5 - Correlation proposed between the “Italcementi active quarry” section and the GSSP Kuhjoch section (Austria) by von Hillebrandt et al. (2007) and Ruhl et al. (2011); St. Audrie’s bay section (UK) by van de Schootbrugge et al. (2007) and Ruhl et al. (2010). Legend of lithological symbols is reported in Fig. 2. TME = Triassic mass extinction

we notice that the FO of *S. punctulata* in the “Italcementi active quarry” section correlates well with the record at Kuhjoch section. The FO of *S. punctulata* at Kuhjoch and St. Audrie’s Bay sections is always lower than the FO of the ammonite *P. spelae* and *P. planorbis* and lower than the acme of *K. reissingeri*, which occurs at similar stratigraphic level in all three sections.

Paleoenvironmental conditions across the TJB interval

The data collected in this study confirm the presence in the western Tethys of the three principal carbon isotope anomalies characterizing the TJB interval and highlight variations in nannofossil abundance, assemblage composition as well as in the size of *P. triassica* (Fig. 6). Some of the variations detected can be correlated with the record from the Northern Calcareous Alps (Austria) by Clémence et

al. (2010) who identified, on the basis of geochemical and micropaleontological data, the occurrence of a multi-phase environmental disruption across the TJB interval. In particular, the authors identified a perturbation phase characterized by three steps (Fig. 6) marked by: a decrease in abundance of *P. triassica* (step 1); predominant medium *P. triassica* (step 2); very low abundance of *P. triassica* and dominance of small-sized specimens (step 3). After step 3, the “initial negative CIE” interval resulted to be barren of nannofossils. In the “Italcementi active quarry” section, no change in nannofossil abundance and assemblage composition was detected across the “precursor CIE” (Figs 3, 6) which was not studied in the Austrian sites (Clémence et al. 2010). In our studied section the interval above the “precursor CIE”, is characterized by very large and abundant *P. triassica* and can be correlated with the pre-perturbation interval of Clémence et

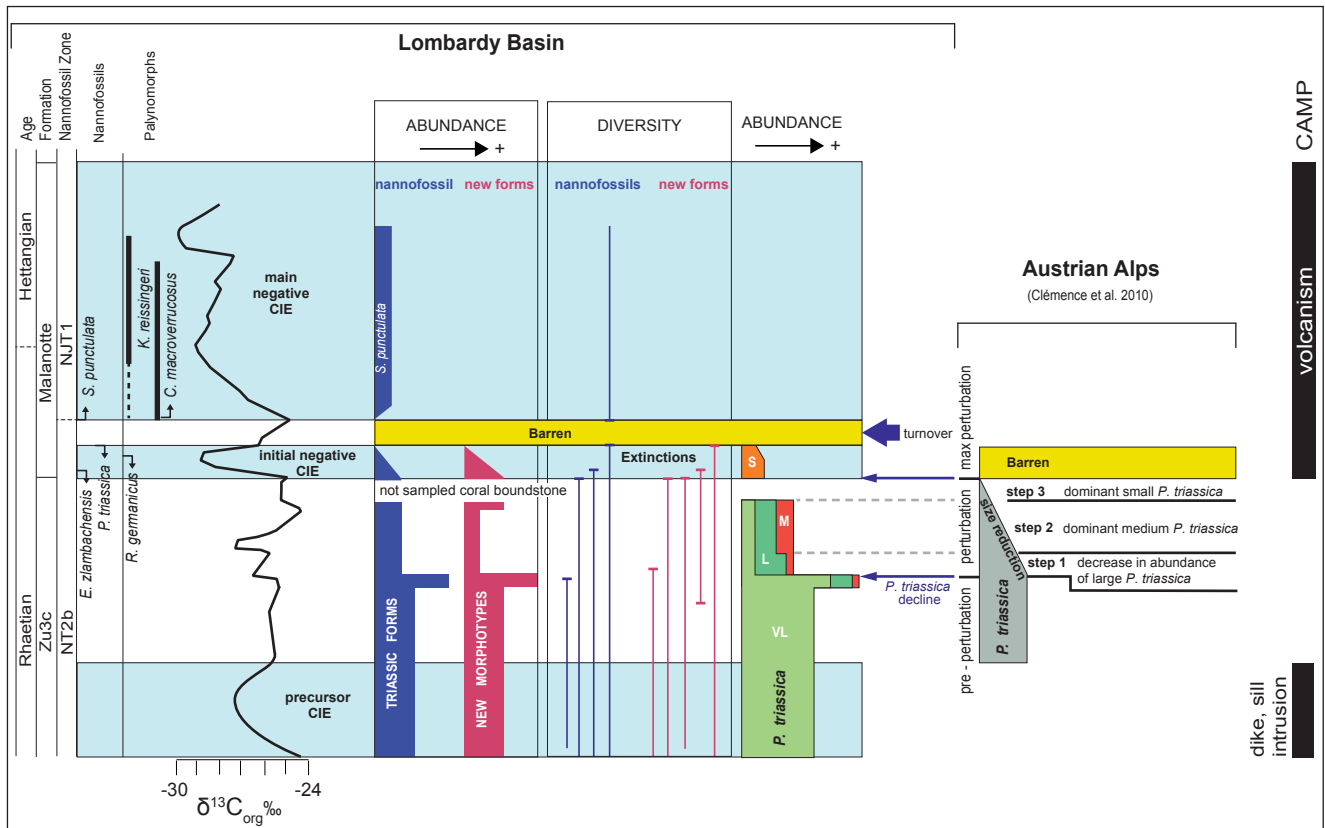


Fig. 6 - Synthesis of calcareous nannofossil biostratigraphy and abundance changes across the TJB interval identified in the Lombardy Basin (this work) correlated with CAMP volcanism (from Cohen & Coe 2002; Kuroda et al. 2010; Ruhl & Kürschner 2011). Palynomorph events are from Galli et al. (2005, 2007). The $\delta^{13}\text{C}_{\text{org}}$ curve is from the “Italcementi active quarry” section (this study). Total abundance and diversity of nannofossils and “new morphotypes” is provided. Distribution and abundance of *P. triassica* morphotypes (S = small, M = medium, L = large, VL = very large) are compared with the record from Northern Calcareous Alps (Clémence et al. 2010) which includes three steps of changes in abundance and size of *P. triassica*.

al. (2010), although they never observed very large morphotypes. In the late part of the pre-perturbation interval, we detected a relative change in nannofossil assemblages, with the FO of morphotype sp. 2 followed, at the top, by the LO of *H. floralis*, FO of large and medium *P. triassica*, and a spike in the nannofossil and “new morphotype” abundances. The spike is followed by the disappearance of morphotype sp. 5 and by a decrease in the abundance of nannofossils, *P. triassica* and “new morphotypes”. The decline in the total abundance of *P. triassica*, paralleled by the occurrence of large- and medium-sized specimens, can be stratigraphically correlated with step 1 of Clémence et al. (2010). The overlying level, marked by a relative decrease of large *P. triassica* and increase of medium *P. triassica*, may be instead correlated with step 2 of Clémence et al. (2010), also characterized by medium *P. triassica* becoming more abundant. Very large-, large- and medium-sized *P. triassica* disappeared at the base of a coral boundstone not sampled for nannofossils.

P. triassica within the “initial negative CIE” is represented exclusively by rare to frequent small specimens. Such assemblage is equivalent of step 3 (of Clémence et al. 2010) although the stratigraphic resolution prevents a precise correlation. The “initial negative CIE” interval is further characterized in the studied section by a steep decrease in the total nannofossil and “new morphotypes” abundances and the stepped extinctions of the Triassic taxa and of the “new morphotypes”. The “initial negative CIE” is followed by barren samples in correspondence of a brief positive carbon isotope excursion. At the onset of the “main negative CIE” *S. punctulata* first occurs and rapidly increases in abundance; this is the only taxon observed in the Malanotte Fm.

The comparison of the datasets from the Northern and Southern Calcareous Alps highlighted similar and coeval variations in abundance and size of *P. triassica* occurring in multiple steps, and provided information regarding the paleoenvironmental changes characterizing the TJB interval. The corre-

spondence between the two records is suggestive for a supraregional significance of the variations detected in nannofossils rather than for an influence of local factors. The TJB interval was the time of the Central Atlantic Magmatic Province (CAMP) activity. Evidence for an initial phase of disturbance of global biogeochemical cycle was provided by Ruhl and Kürschner (2011). They suggested that, across the “precursor negative CIE”, some 100 kys prior to the “initial negative CIE” (Deenen et al. 2010), the intrusion by dike and sill systems could have released large amounts of volatiles (e.g., CH₄, CO₂, and likely SO₂) from subsurface organic-rich sediments.

A large and rapid CO₂ release was suggested to have occurred in correspondence of the “initial negative CIE” due to outgassing during the CAMP extrusive volcanic activity and, possibly, the addition of isotopically light carbon from gas hydrates (Marzoli et al. 1999; Pálffy et al. 2001; Ward et al. 2001; Hesselbo et al. 2002; Cohen & Coe 2002, 2007; Huynh & Poulsen 2005; Galli et al. 2005; Kuroda et al. 2010; Ruhl et al. 2011; Blackburn et al. 2013; Jaraula et al. 2013; Shaller et al. 2015). It was a relatively short-lived event, that occurred within ~20 to 40 kyrs (Ruhl et al. 2011) and had a profound impact on global climate and ocean chemistry, as suggested by palynological data showing increased humidity coinciding with the onset of the “initial negative CIE” (Kürschner et al. 2007; van de Schootbrugge et al. 2009). In the Lombardy Basin, this interval, coincides with the first ca. 2.6 meters of the Malanotte Fm., suggestive for a dramatic change in the paleoconditions towards relatively deeper paleodepth and increased terrigenous input (Galli et al. 2005, 2007). Evidence, on a global scale, for increasing *p*CO₂ across the TJB interval was provided by Beerling (2002), Beerling and Berner (2002) and Berner and Beerling (2006). Kasprak et al. (2015) reconstructed a severe change in ocean redox state and nutrient cycling across the “initial negative CIE”, addressed as the potential mechanism inducing the marine and terrestrial assemblage-changes and extinctions detected worldwide. Guex et al. (2016), suggested that the biotic crisis was probably associated with initial thermal erosion of the cratonic lithosphere due to emplacement of the CAMP leading to emission of sulfur causing global cooling. The release of destructive toxic compounds and gasses, as SO₂, was addressed as a possible trigger

for the end-Triassic mass extinction by several authors (e.g., Self et al. 2006; Ganino and Arndt 2009; van de Schootbrugge et al. 2009).

Variations in nannofossil assemblage composition, abundance and size of *P. triassica* suggest that a major change in paleoceanographic conditions occurred after the “precursor negative CIE” and before the “initial negative CIE”. The detected patterns are suggestive for a progressive decline of biogenic calcite production, expressed by a decrease in abundance and smaller specimens of *P. triassica*, possibly induced by changes in climatic and surface-water chemical conditions, including increased fertility and excess CO₂ in the ocean/atmosphere system. The identification of subsequent steps in nannofloral modifications is perhaps suggestive for multiple and distinctive phases of CAMP volcanism. Moreover, changes in calcareous nannoplankton unequivocally indicate that early pulses started to affect marine surface-water prior to the climax perturbation of the “initial negative CIE” that induced the turnover from Triassic to Jurassic taxa. The stepped extinction of nannofossils during the “initial negative CIE” indicates that calcareous nannoplankton suffered the most adverse paleoceanographic conditions progressively eliminating the most tolerant taxa. Our findings indicate that *P. triassica* could survive longer being probably the most resistant taxon although forced to produce smaller exoskeleton.

The turnover from Triassic nannofloras to Jurassic assemblages began under continuing perturbed conditions associated to the CAMP volcanism (e.g., Pálffy et al. 2001; Ward et al. 2001; Hesselbo et al. 2002; Kürschner et al. 2007; Cohen & Coe 2002, 2007; Huynh & Poulsen 2005; Galli et al. 2005; Kuroda et al. 2010; van de Schootbrugge et al. 2009; Guex et al. 2004, 2016). The FO of *S. punctulata* correlated with the onset of the “main negative CIE”, as previously documented in other sections (von Hillebrandt et al. 2007; van de Schootbrugge et al. 2007), in the interval of radiation of Jurassic taxa of other groups (e.g., ammonites, radiolarians, palynomorphs) (Hallam & Wignall 1997; Galli et al. 2005, 2007; Kürschner et al. 2007; van de Schootbrugge et al. 2009; McRoberts et al. 2012).

The progressive deterioration of calcareous nannoplankton across the TJB interval, shows some pattern resembling those detected across the Toarcian-Oceanic Anoxic Event (T-OAE) and the early Aptian OAE 1a: in fact, both OAEs were preceded

by a stepped decline in abundance of heavily calcified forms (schizosphaerellids in the Toarcian and nannoconids in the latest Barremian-early Aptian) resulting from the combination of changes in surface-water fertility and progressive ocean acidification induced by Large Igneous Province (LIP) emplacement (Erba 2004). Since *P. triassica* was the most calcified nannofossil in the Late Triassic, it might well be that its paleoecological affinities were similar to those of *S. punctulata* and nannoconids. Consequently, LIP-induced fertilization and acidification stressed the potentially oligotrophic *P. triassica* that, under excess CO₂ in the ocean/atmosphere system, reduced calcification diminishing the number and the size of specimens.

Although the paleoenvironmental disruption in the TJB interval is similar to later ecosystem perturbations across T-OAE and OAE 1a, the “initial negative CIE” nannofossil turnover represents a very different evolutionary mode. In fact, across T-OAE and OAE 1a major originations phases derived from appearance of many new species in absence of any extinction. We speculate that Triassic nannoplankton was probably less able to adapt being at an early stage of evolution.

CONCLUSION

The new data presented in this work and their correlation with the available datasets for the TJB interval revealed, for the first time, latest Triassic nannofossils in the Lombardy Basin, and allowed the age determination of the upper Zu Limestone and the Malanotte fms. The TJB falls in the lowermost part of the NJT1 nannofossil bio-zone and the lowermost part of the Malanotte Fm. Two nannofossil events resulted to be reliable markers to constrain the TJB interval: the LO of *P. triassica* and the FO of *S. punctulata*. In addition, new morphotypes documented in the Rhaetian, implemented the characterization of the Late Triassic assemblages and, their disappearance, might constitute a further element for the characterization of the mass-extinction in the TJB boundary interval.

A decrease in size and abundance of *P. triassica* occurred soon after the “precursor CIE” and was paralleled by a decline in the total nannofossil abundance which culminated with a stepped extinction of Triassic nannofossils within the “initial negative

CIE”. The data are suggestive for an early perturbation on nannoplankton biocalcification which occurred before the extinction possibly testifying initial pulses of the CAMP LIP. The progressive decline of biogenic calcite production, expressed by a decrease in abundance and production of smaller specimens of *P. triassica*, was possibly resulting from the combination of changes in surface-water fertility and progressive ocean acidification, both presumably induced by the CAMP volcanism. The disappearance of Triassic taxa seem to be coincident with massive emplacement of CAMP flood basalts triggering a global climate change and alteration of the oceanic carbonate system. Triassic nannofossils show at least two steps of extinctions with *P. triassica* surviving longer. After the mass extinction, the regaining of calcareous phytoplankton is represented by the appearance of *S. punctulata* at the onset of the “main negative CIE”. Although the latest Triassic decline in calcite production resembles patterns documented across the T-OAE and OAE 1a, the complete turnover from Triassic to Jurassic taxa is peculiar of the TJB interval. Indeed, the extinctions of Triassic nannoplankton might derive from the juvenile stage of this group in its evolutionary history. The appearance of new taxa under highly perturbed conditions was also documented for other paleoenvironmental anomalies such as Jurassic and Cretaceous OAEs. The micropaleontological record suggests that calcareous nannoplankton could rapidly react to extreme stressing conditions with production of new forms of exoskeleton.

Acknowledgments. MR and MZ were supported by Faculty project funds PRAT Rigo, CPDA152211/15 (University of Padova). The paper benefited of the thoughtful comments of two anonymous reviewers.

REFERENCES

- Bachan A., Schootbrugge B., Fiebig J., McRoberts C.A., Ciarpica G. & Payne J.L. (2012) - Carbon cycle dynamics following the end-Triassic mass extinction: Constraints from paired $\delta^{13}\text{C}_{\text{carb}}$ and $\delta^{13}\text{C}_{\text{org}}$ records. *Geochem., Geophys., Geosyst.*, 13(9).
- Beerling D.J. (2002) - Palaeoclimatology. CO₂ and the end-Triassic mass extinction *Nature*, 415: 386–387
- Beerling D.J. & Berner R.A. (2002) - Biogeochemical constraints on the Triassic-Jurassic boundary carbon cycle event.

Global Biogeochemical Cycles, 16(3).

- Bellanca A., Di Stefano E., Di Stefano P., Erba E., Neri R. & Pirini Radrizzani C. (1993) - Ritrovamento di "Calcisfere" e nanofossili calcarei in terreni carnici della Sicilia. *Palaeopelagos*, 3: 91-96.
- Bellanca A., Di Stefano P. & Neri R. (1995) - Sedimentology and isotope geochemistry of Carnian deep-water marl/limestone deposits from the Sicani Mountains, Sicily: Environmental implications and evidence for a planktonic source of lime mud. *Palaeogeogr., Palaeoclimatol., Palaeoecol.*, 114(1): 111-129.
- Berner R. A. & Beerling D.J. (2007) - Volcanic degassing necessary to produce a CaCO₃ undersaturated ocean at the Triassic-Jurassic boundary. *Palaeogeogr., Palaeoclimatol., Palaeoecol.*, 244(1): 368-373.
- Berra F., Jadoul F. & Anelli A. (2010) - Environmental control on the end of the Dolomia Principale/Hauptdolomiti depositional system in the Central Alps: coupling sea-level and climatic changes. *Palaeogeogr., Palaeoclimatol., Palaeoecol.*, 290: 138-150.
- Bertotti, G., Picotti V., Bernoulli D. & Castellarin A. (1993) - From rifting to drifting: tectonic evolution of the South-Alpine upper crust from the Triassic to the Early Cretaceous. *Sediment. Geol.*, 86: 53-76.
- Blackburn T.J., Olsen P.E., Bowring S.A., McLean N.M., Kent D.V., Puffer J., McHone G., Rasbury E.T. & Et-Touhami M. (2013) - Zircon U-Pb geochronology links the end-Triassic extinction with the Central Atlantic Magmatic Province. *Science*, 340: 941-945.
- Bonis N.R., Ruhl M. & Kürschner W.M. (2010) - Climate change driven black shale deposition during the end-Triassic in the western Tethys. *Palaeogeogr., Palaeoclimatol., Palaeoecol.*, 290(1): 151-159.
- Bown P.R. (1987) - The structural development of Early Mesozoic coccolith and its evolutionary and taxonomic significance. *Abh Geol. B. A.*, 39: 33-49.
- Bown P.R., (1998) - Triassic. In: Bown P.R. (Ed.) - Calcareous nanofossil biostratigraphy: 29-33. British Micropalaeontological Society Publication Series, Chapman & Hall.
- Bown P.R. & Young J.R. (1998) - Techniques. In: P.R. Bown (Ed.) - Calcareous nanofossil biostratigraphy. London: British Micropalaeontological Society Series, Chapman and Hall/Kluwer Academic Press.
- Bralower T.J., Bown P.R. & Siesser W.G. (1991) - Significance of upper Triassic nanofossils from the southern hemisphere (ODP Leg 122, Wombat Plateau, NW Australia). *Mar. Micropaleontol.*, 17(1): 119-154.
- Bralower T.J., Bown P.R. & Siesser W.G. (1992) - Upper Triassic Calcareous nanoplankton biostratigraphy, Wombat Plateau, Northwest Australia. Proceedings of the Ocean Drilling Program, Scientific Results, Vol. 122.
- Clémence M.E., Bartolini A., Gardin S., Paris G., Beaumont V., & Page K.N. (2010) - Early Hettangian benthic-planktonic coupling at Doniford (SW England): Palaeoenvironmental implications for the aftermath of the end-Triassic crisis. *Palaeogeogr., Palaeoclimatol., Palaeoecol.*, 295(1): 102-115.
- Cohen A.S. & Coe A.L. (2002) - New geochemical evidence for the onset of volcanism in the Central Atlantic magmatic province and environmental change at the Triassic-Jurassic boundary. *Geology*, 30(3): 267-270.
- Coplen T.B., Brand W.A., Gehre M., Groning M., Meijer H.A.J., Toman B. & Verkouteren R.M. (2006) - New guidelines for $\delta^{13}\text{C}$ measures. *Analytical Chemistry*, 78: 2439-2441.
- Deenen M.H., Ruhl M., Bonis N.R., Krijgsman W., Kuerschner W. M., Reitsma M. & Van Bergen M. J. (2010) - A new chronology for the end-Triassic mass extinction. *Earth Planet. Sci. Lett.*, 291(1): 113-125.
- Di Nocera S. & Scandone P. (1977) - Triassic nanoplankton limestones of deep basin origin in the central Mediterranean region. *Palaeogeogr., Palaeoclimatol., Palaeoecol.*, 21: 101-111.
- Erba E. (1994) - Nanofossils and superplumes: the early Aptian nannoconid crisis. *Paleoceanography*, 9: 483-501.
- Erba E. (2004) - Calcareous nanofossils and Mesozoic oceanic anoxic events. *Mar. Micropaleontol.*, 52: 85-106.
- Erba E. & Tremolada F. (2004) - Nanofossil carbonate fluxes during the Early Cretaceous: phytoplankton response to nutrification episodes, atmospheric CO₂ and anoxia. *Paleoceanography*, 19. doi:10.1029/2003PA000884.
- Erba E., Castradori D. & Cobianchi M. (1992) - Compilation of Upper Triassic and Jurassic calcareous nanofossil ranges. *Mem. Sci. Geol.*, 43: 27-40.
- Erba E. (2006) - The first 150 million years history of calcareous nanoplankton: Biosphere-geosphere interactions. *Palaeogeogr., Palaeoclimatol., Palaeoecol.*, 232: 237-250.
- Erba E., Bottini C., Weissert J.H. & Keller C.E. (2010) - Calcareous Nanoplankton Response to Surface-Water Acidification Around Oceanic Anoxic Event 1a. *Science*, 329: 428-432.
- Felber R., Weissert H.J., Furrer H. & Bontognali T.R. (2015) - The Triassic-Jurassic boundary in the shallow-water marine carbonates from the western Northern Calcareous Alps (Austria). *Swiss J. Geosci.*, 108(2-3): 213-224.
- Galli M.T., Jadoul F., Bernasconi S.M. & Weissert H. (2005) - Anomalies in global carbon cycling and extinction at the Triassic/Jurassic boundary: evidence from a marine C-isotope record. *Palaeogeogr., Palaeoclimatol., Palaeoecol.*, 216(3): 203-214.
- Galli M. T., Jadoul F., Bernasconi S. M., Cirilli S. & Weissert H. (2007) - Stratigraphy and palaeoenvironmental analysis of the Triassic-Jurassic transition in the western Southern Alps (Northern Italy). *Palaeogeogr., Palaeoclimatol., Palaeoecol.*, 244(1): 52-70.
- Ganino C. & Arndt N.T. (2009) - Climate changes caused by degassing of sediments during the emplacement of large igneous provinces. *Geology*, 37: 323-326.
- Gardin S., Krystyn L., Richoz S., Bartolini A. & Galbrun B. (2012) - Where and when the earliest coccolithophores? *Lethaia*, 45(4): 507-523.
- Gnaccolini M. (1965) - Calcarea di Zu e Argilliti di Riva di Solto: due formazioni del Retico Lombardo. *Riv. It. Paleontol. Stratigr.*, 71: 1099-1121.
- Guex J., Bartolini A., Atudorei V. & Taylor D. (2003) - Two negative $\delta^{13}\text{C}_{\text{org}}$ excursions near the Triassic-Jurassic boundary in the New York Canyon area (Gabbs Valley Range, Nevada). *Bull. Soc. vandoise sci. nat.*, 88(4): 445-448.

- Guex J., Bartolini A., Atudorei V. & Taylor D. (2004) - High-resolution ammonite and carbon isotope stratigraphy across the Triassic–Jurassic boundary at New York Canyon (Nevada). *Earth Planet. Sci. Lett.* 225: 29–41.
- Guex J., Pilet S., Müntener O., Bartolini A., Spangenberg J., Schoene B., Sell B. & Schaltegger U. (2016) - Thermal erosion of cratonic lithosphere as a potential trigger for mass-extinction. *Scientific Reports*, 6. DOI: 10.1038/srep23168.
- Hallam A. & Wignall P.B. (1997) - Mass extinction and sea level change. *Earth-Sci. Rev.*, 48: 217–258.
- Hallam A. (2002) - How catastrophic was the end-Triassic mass extinction? *Lethaia*, 35(2): 147–157.
- Hesselbo S.P., Robinson S.A., Surlyk F. & Piasecki S. (2002) - Terrestrial and marine extinction at the Triassic–Jurassic boundary synchronized with major carbon-cycle perturbation: a link to initiation of massive volcanism? *Geology*, 30: 251–254.
- Huynh T.T. & Poulsen C.J. (2005) - Rising atmospheric CO₂ as a possible trigger for the end-Triassic mass extinction. *Palaeogeogr., Palaeoclimatol., Palaeoecol.*, 217(3): 223–242.
- Jadoul F., Berra F. & Frisia S. (1992) - Stratigraphic and paleogeographic evolution of a carbonate platform in an extensional tectonic regime: the example of the Dolomia Principale in Lombardy (Italy). *Riv. It. Paleontol. Stratigr.*, 98: 29–44.
- Jadoul F., Masetti, D., Cirilli, S., Berra, F., Claps, M. & Frisia, S. (1994) - Norian–Rhaetian stratigraphy and paleogeographic evolution of the Lombardy Basin (Bergamasc Alps): Excursion B1, 15th IAS Regional Meeting: 5–38.
- Jadoul F., Galli M.T., Berra F., Cirilli S., Ronchi P. & Paganoni A. (2004) - The Late Triassic–Early Jurassic of the Lombardy Basin: stratigraphy, palaeogeography and palaeontology. *32nd Int. Geol. Congr., Field Trip Guide Book P68*, vol. 6. 36 pp.
- Jadoul F., Calabrese L., Galli M.T. & Gnaccolini M. (2005) - Rhaetian–Early Sinemurian carbonate platforms in western Lombardy (Varese, Southern Alps, Italy): stratigraphical and paleogeographical implications. *Riv. It. Paleontol. Stratigr.*, 111(2): 285–303.
- Jadoul F., Galli M.T., Muttoni G., Rigo M. & Cirilli S. (2012) - The late Norian–Hettangian stratigraphic and paleogeographic evolution of the Bergamasc Alps. Escursione pre congresso Geoitalia, VI meeting FIST - Rimini, 2007. *Geol.F. Trips*, Vol. 4 No.1.1 (2012), 55 pp., 22 figs. (DOI 10.3301/GFT.2012.01)
- Jadoul F. & Galli M.T. (2008) - The Hettangian shallow water carbonates after the Triassic/Jurassic biocalcification crisis: the Albenza Formation in the Western Southern Alps. *Riv. It. Paleontol. Stratigr.*, 114(3): 453–470.
- Jafar S.A. (1983) - Significance of Late Triassic calcareous nannoplankton from Austria and southern Germany. *Neues Jahrb. Geol. Paläontol., Abh.*, 166(2): 218–259.
- Janofske D. (1987) - Kalkige Nannofossilien aus der Ober-Trias (Rhät) der Nördlichen Kalkalpen. *Berliner Geowiss. Abh.*, A, 86: 45–67.
- Janofske D. (1992) - Calcareous nannofossils of the Alpine upper Triassic. *Nannoplankton res.*, 1: 87–109.
- Jaraula C.M., Grice K., Twitchett R.J., Böttcher M.E., LeMetayer P., Dastidar A.G. & Opazo L.F. (2013) - Elevated pCO₂ leading to Late Triassic extinction, persistent photic zone euxinia, and rising sea levels. *Geology*, 41(9): 955–958.
- Kasprak A.H., Sepúlveda J., Price-Waldman R., Williford K.H., Schoepfer S.D., Haggart J.W., Ward P.D., Summons R.E. & Whiteside J.H. (2015) - Episodic photic zone euxinia in the northeastern Panthalassic Ocean during the end-Triassic extinction. *Geology*, 43(4): 307–310.
- Kürschner W.M., Bonis N.R. & Krystyn L. (2007) - Carbon-isotope stratigraphy and palynostratigraphy of the Triassic–Jurassic transition in the Tiefengraben section–Northern Calcareous Alps (Austria). *Palaeogeogr., Palaeoclimatol., Palaeoecol.*, 244(1): 257–280.
- Kuroda J., Hori R.S., Suzuki K., Gröcke D.R. & Ohkouchi N. (2010) - Marine osmium isotope record across the Triassic–Jurassic boundary from a Pacific pelagic site. *Geology*, 38(12): 1095–1098.
- Lakew T. (1990) - Microfacies and cyclic sedimentation of the Upper Triassic (Rhaetian) Zu Limestone (Southern Alps). *Facies*, 22: 187–232.
- Marzoli A., Renne P.R., Piccirillo E.M., Ernesto A., Bellieni G. & De Min A. (1999) - Extensive 200-million-year-old continental flood basalts of the central Atlantic magmatic province. *Science* 284: 616–618.
- Mattioli E. & Erba E. (1999) - Synthesis of calcareous nannofossil events in Tethyan Lower and Middle Jurassic successions. *Riv. It. Paleontol. Stratigr.*, 105(3): 343–376.
- McRoberts C.A. (1994) - The Triassic–Jurassic ecostratigraphic transition in the Lombardian Alps, Italy. *Palaeogeogr., Palaeoclimatol., Palaeoecol.*, 110: 145–166.
- McRoberts C.A., Furrer H. & Jones D.S. (1997) - Palaeoenvironmental interpretation of a Triassic–Jurassic boundary section from Western Austria based on palaeoecological and geochemical data. *Palaeogeogr., Palaeoclimatol., Palaeoecol.*, 136: 79–95.
- McRoberts C.A., Krystyn L. & Hautmann M. (2012) - Macrofaunal response to the end-Triassic mass extinction in the West-Tethyan Kössen Basin, Austria. *Palaios*, 27(9): 607–616.
- McElwain J.C., Beerling D.J. & Woodward F.I. (1999) - Fossil plants and global warming at the Triassic–Jurassic boundary. *Science*, 285: 1386–1390.
- Monechi S. & Thierstein H. (1985) - Late Cretaceous–Eocene nannofossil and magnetostratigraphic correlations near Gubbio, Italy. *Mar. Micropaleontol.*, 9: 419–440.
- Moshkovitz S. (1982) - On the findings of a new calcareous nannofossil (*Conusphaera zambachensis*) and other calcareous organisms in the Upper Triassic sediments of Austria. *Eclogae geol. Helv.*, 75(3): 611–619.
- Muttoni G., Kent D. V., Jadoul F., Olsen P. E., Rigo M., Galli M. T. & Nicora A. (2010) - Rhaetian magneto-biostratigraphy from the Southern Alps (Italy): constraints on Triassic chronology. *Palaeogeogr., Palaeoclimatol., Palaeoecol.*, 285(1): 1–16.
- Newell N.D. (1963) - Crises in the history of life. *Sci. Am.*, 208: 76–92.
- Noel D. (1965) - Sur les coccoliths du Jurassique européen et

- d'Afrique du Nord. Essai de classification des coccolithes fossiles. Edition du Centre national de la Recherche Scientifique. Paris, 209 pp.
- Olsen P.E., Kent D.V., Sues H.-D., Koeberl C., Huber H., Montanari A., Rainforth E.C., Fowell S.J., Szajina M.J. & Hartline B. (2002) - Ascent of dinosaurs linked to an iridium anomaly at the Triassic-Jurassic boundary. *Science*, 296: 1305-1307.
- Onoue T. & Sano H. (2007) - Triassic mid-oceanic sedimentation in Panthalassa Ocean: Sambosan accretionary complex, Japan. *Island Arc*, 16(1): 173-190.
- Pálffy J., Demény A., Haas J., Hetényi M., Orchard M.J. & Vető I. (2001) - Carbon isotope anomaly and other geochemical changes at the Triassic-Jurassic boundary from a marine section in Hungary. *Geology*, 29: 1047-1050.
- Preto N., Rigo M., Agnini C., Bertinelli A., Guaiumi C., Borello S. & Westphal H. (2012) - Triassic and Jurassic calcareous nannofossils of the Pizzo Mondello section: a SEM study. *Riv. It. Paleontol. Stratigr.*, 118(1): 131-141.
- Preto N., Willems H., Guaiumi C. & Westphal H. (2013a) - Onset of significant pelagic carbonate accumulation after the Carnian Pluvial Event (CPE) in the western Tethys. *Facies*, 59(4): 891-914.
- Preto N., Agnini C., Rigo M., Sprovieri M. & Westphal H. (2013b) - The calcareous nannofossil *Prinsiosphaera* achieved rock-forming abundances in the latest Triassic of western Tethys: consequences for the $\delta^{13}\text{C}$ of bulk carbonate. *Biogeosciences*, 10(9): 6053-6068.
- Prins B. (1969) - Evolution and stratigraphy of coccolithinids from the Lower and Middle Lias. Proc. 1st Int. Conf. Planktonic Microfossils, Geneva, 2: 547-558.
- Raup D.M. & Sepkoski J. J. (1984) - Periodicity of extinctions in the geologic past. *Proc. Nat. Acad. Sci.*, 81(3): 801-805.
- Ridgwell A. & Zeebe R. E. (2005) - The role of the global carbonate cycle in the regulation and evolution of the Earth system. *Earth Plan. Sci. Lett.*, 234(3): 299-315.
- Rigo M., Galli M.T. & Jadoul F. (2009) - Late Triassic biostratigraphic constraints in the Imagna Valley (western Bergamasco Alps, Italy). *Albertiana*, 37: 39-42.
- Ruhl M. & Kürschner W. M. (2011) - Multiple phases of carbon cycle disturbance from large igneous province formation at the Triassic-Jurassic transition. *Geology*, 39(5): 431-434.
- Ruhl M., Kürschner W.M. & Krystyn L. (2009) - Triassic-Jurassic organic carbon isotope stratigraphy of key sections in the western Tethys realm (Austria): *Earth Plan. Sci. Lett.*, 281: 169-187, doi: 10.1016/j.epsl.2009.02.020.
- Ruhl M., Deenen M.H.L., Abels H.A., Bonis N.R., Krijgsman W. & Kürschner W.M. (2010) - Astronomical constraints on the duration of the Early Jurassic Hettangian stage and recovery rates following the end-Triassic mass extinction (St Audrie's Bay/East Quantoxhead, UK). *Earth Plan. Sci. Lett.*, 295: 262-276, doi: 10.1016/j.epsl.2010.04.008.
- Ruhl M., Bonis N.R., Reichart G.J., Sinninghe Damsté J.S. & Kürschner W.K. (2011) - Atmospheric Carbon Injection Linked to End-Triassic Mass Extinction. *Science*, 333: 430-433. doi: 10.1126/science.1204255
- Schaller M. F., Wright J. D. & Kent D. V. (2015) - A 30 Myr record of Late Triassic atmospheric $p\text{CO}_2$ variation reflects a fundamental control of the carbon cycle by changes in continental weathering. *Geol. Soc. America Bull.*, 127(5-6): 661-671.
- Self S., Widdowson M., Thordarson T. & Jay A.E. (2006) - Volatile fluxes during flood basalt eruptions and potential effects on the global environment: A Deccan perspective. *Earth Plan. Sci. Lett.*, 248(1): 518-532.
- Spotl C. & Vennemann T.W. (2003) - Continuous-flow isotope ratio mass spectrometric analysis of carbonate minerals. *Rapid Commun. Mass Spectrom.*, 17: 1004-1006. doi: 10.1002/rcm.1010
- Tanner L.H., Lucas S.G. & Chapman M.G. (2004) - Assessing the record and causes of Late Triassic extinctions. *Earth-Sci. Rev.*, 65: 103-139.
- Trotter J. A., Williams I.S., Nicora A., Mazza M. & Rigo M. (2015) - Long-term cycles of Triassic climate change: a new $\delta^{18}\text{O}$ record from conodont apatite. *Earth Plan. Sci. Lett.*, 415: 165-174.
- Van de Schootbrugge B., Tremolada F., Rosenthal Y., Bailey T. R., Feist-Burkhardt S., Brinkhuis H., Pross J., Kent D.V. & Falkowski P. G. (2007) - End-Triassic calcification crisis and blooms of organic-walled 'disaster species'. *Palaeogeogr., Palaeoclimatol., Palaeoecol.*, 244(1): 126-141
- Van de Schootbrugge B., Payne J.L., Tomasovych A., Pross J., Fiebig J., Benbrahim M., Föllmi K.B. & Quan T. M. (2008) - Carbon cycle perturbation and stabilization in the wake of the Triassic-Jurassic boundary mass-extinction event. *Geochem., Geophys., Geosyst.*, 9(4).
- Van de Schootbrugge B., Quan T.M., Lindström S., Püttmann W., Heunisch C., Pross J., Fiebig J., Petschick R., Röhling H.-G., Richoz S., Rosenthal & Y. P. Falkowski G. (2009) - Floral changes across the Triassic/Jurassic boundary linked to flood basalt volcanism. *Nature Geosci.*, 2(8): 589-594.
- Von Hillebrandt A.V., Krystyn L. & Kürschner, W.M. (2007) - A candidate GSSP for the base of the Jurassic in the northern Calcareous Alps (Kuhjoch section; Karwendel Mountains, Tyrol, Austria). *ISJS Newsletter*, 34(1): 2-20.
- Ward P.D., Haggart J.W., Carter E.S., Wilbur D., Tipper H.W. & Evans T. (2001) - Sudden productivity collapse associated with the Triassic-Jurassic boundary mass-extinction. *Science*, 292: 2185-2188.
- Ward P.D., Garrison G.H., Haggart J.W., Kring D.A. & Beattie M.J. (2004) - Isotopic evidence bearing on Late Triassic extinction events, Queen Charlotte Islands, British Columbia, and implications for the duration and cause of the Triassic/Jurassic mass extinction. *Earth Plan. Sci. Lett.*, 224: 589-600.
- Whiteside J. H., Grogan D. S., Olsen P. E. & Kent D.V. (2011) - Climatically driven biogeographic provinces of Late Triassic tropical Pangea. *Proc. Nat. Acad. Sci.*, 108(22): 8972-8977.

APPENDIX I

Table reporting Carbon stable-isotope data for bulk carbonate and bulk organic carbon fractions for samples from the “Italcementi active quarry” section.

Sample	m	$\delta^{13}\text{C carb}$	$\delta^{18}\text{O carb}$	$\delta^{13}\text{C org}$
j28	98	4.4772	-2.0016	nd
j 27	95	0.8246	-5.6852	-27.0280
j 26	91.5	2.5752	-4.4692	-27.6496
j 25	90	2.4740	-2.8379	-27.0890
j 24	87	2.4553	-2.1426	-27.7921
j 23	86.5	1.9032	-3.1224	-26.8100
j 22	84.5	3.3107	-2.6415	-27.5069
j 21	82.5	3.3973	-2.9912	-28.6267
j 20	81.8	2.8171	-5.9972	-28.2114
j 19	81	3.6772	-2.7771	-27.9932
j 18	80.5	3.6992	-3.0599	-27.4117
j 16	76.5	3.3054	-3.9136	-27.5749
j 15	75.4	1.3166	-4.9619	-26.7589
j 13	73.4	3.5940	-1.8408	-26.5029
j 11	72.5	-1.9493	-6.3512	-26.8209
j 9	71.6	0.8805	-6.1348	-26.7138
j 7	71.2	2.5620	-2.7879	-28.7251
j 5	70.4	-0.0359	-5.4685	-27.4497
j 4	70.2	-0.7829	-4.0425	-27.7996
j 3	70	-0.5835	-6.8591	-27.8974
j7/12	69.8	0.1832	-4.7873	-26.5152
j 2	66.5	2.5025	-2.3052	-27.7829
zu 1	58.8	2.8068	-1.3305	-26.2429
zu 2	57.2	-1.4443	-5.7029	-27.0720
zu 3	54.4	2.1732	-2.6800	-29.4542
zu 4	54.2	2.3817	-2.2900	-25.9915
zu 5	53.5	2.3365	-2.7700	-26.3041
zu 6	50.4	3.0373	-2.8061	-24.9154
zu 8	49.8	2.8379	-1.6300	-25.1729
zu9	49.7	3.4602	-1.1987	-24.9570
zu 10	49.5	2.4048	-2.7500	-25.6682
zu 11	48.5	2.3232	-4.9581	-25.8420
zu 12	48	2.8817	-1.8628	-26.3837
zu 13	45.4	2.2219	-5.1862	-27.0779
zu 14	44.2	2.1255	-1.1203	-26.6639
zu 15	42	2.2245	-2.1800	-26.8811
zu15b	41	2.4071	-1.8086	-25.9582
zu 16	32	2.2844	-1.5016	-26.4039
zu 17	28.5	2.5155	-1.6082	-26.7691
J 01/12	26.5	3.3665	-1.7625	-25.5278
zu 18	26	2.8668	-3.2100	-25.1671
zu 19	23.8	3.3827	-2.5539	-25.9528
zu 20	21.8	2.5744	-4.5000	-28.3664
zu 21	18.8	1.3233	-2.4000	-26.6407
zu 22	15.4	2.2440	-5.3055	-27.3947
zu 23	8.1	1.5741	-3.2987	nd
zu 24	7.5	1.3942	-2.3781	-26.2524
zu 25	6.2	1.5100	-3.4800	-25.4209
zu 26	3.8	1.9381	-2.2400	-25.6383
zu 27	3.4	-3.5857	-3.0063	-26.3550
zu 28	0.1	1.3324	-2.9770	-25.1648

APPENDIX II

Taxonomic index of calcareous nannofossil taxa reported in this study.

Archaeozygodiscus koessensis Bown, 1985

Crucirhabdus minutus Jafar, 1983

Crucirhabdus primulus Prins, 1969 ex Rood et al., 1973, emend Bown, 1987

Eoconusphaera zambachensis (Moshkovitz, 1982) Kristan-Tollmann, 1988

Hayococcus floralis Jafar, 1983

Prinsiosphaera triassica Jafar, 1983

Schizosphaerella punctulata Deflandre & Dangeard, 1938

Tetralithus cassianus Jafar, 1983

Tetralithus pseudotrifidus Jafar, 1983

APPENDIX III

In this appendix a description of unknown nannofossil morphotypes identified in the “Italcementi active quarry” section is provided.

Tetralithus sp. is a nannolith constituted by four rays with relatively long free length (ca. 5-8 μm). It differs from *T. cassianus* since the sutures join in the centre of the nannolith delimiting 4 rays.

Morphotype sp. 1 is a 1 to 3 μm nannolith, composed of four elements that are blocky to rays-like. Sutures are parallel to the outline. Under light microscope colours are light grey to whitish.

Morphotype sp. 2 is a slightly oval to subcircular nannolith (10-15 μm diameter) made of elongated crystals disposed radially around a center sometimes filled by small rhombohedral crystals (less than 1 μm). Morphotype sp. 2 shows the same features of the calcisphere described by Bellanca et al. (1993) and by Preto et al. (2013a) (figures 8a to 8b of Preto et al. 2013a) in the Carnian of Pizzo Mondello (Sicily, Italy) and Pignola-Abriola sections (Lagonegro Basin, southern Italy).

Morphotype sp. 3 is a calcisphere, ca. 10 to 15 μm in diameter, with a smooth regular outline. It is made by usually 6 sub-triangular elements that appear slightly imbricated. Under crossed nicols this morphotype is characterized by high colours.

Morphotype sp. 4 is an elliptical coccolith, of ca. 7-8 μm length and ca. 4-6 μm width, with an open central area sometimes filled with a single calcite crystal.

Morphotype sp. 5 is an elliptical coccolith (2-3 μm in length) with a very narrow rim and large open central area. Specimens resemble *Archaeozygodiscus koessensis* of (Bown, 1985) and coccolith sp. of Gardin et al. (2012).

APPENDIX IV

Calcareous nannofossil range chart of the "Italcementi active quarry" section. The chart reports the quantitative abundance of all taxa and "new morphotypes" observed in smear slides and thin sections.

m	Sample	smear slide (#/900 fields of view)																thin section (#/50 fields of view)			
		<i>E. zimbabachensis</i>	<i>P. triassica</i> very large	<i>Crucirhabdus</i> sp. cf. <i>C. minutus</i>	<i>H. floralis</i>	<i>P. triassica</i> large	<i>P. triassica</i> medium	<i>P. triassica</i> small	<i>S. punctulata</i>	sp. 1	sp. 4	sp. 5	sp. 2	sp. 3	<i>T. cassianus</i>	<i>Tetralithus</i> sp.	Total nannofossil abundance	Total "new forms" abundance	<i>P. triassica</i>	sp. 3	sp. 2
98	j28							4								4	0				
90	j 25							5								5	0				5
84.5	j 22							5								5	0				
81	j 19							4								4	0				4
76.5	j 16							3								3	0				4
75.4	j 15							3								3	0				
73.4	j 13							2								2	0				3
72.5	j 11	barren														0	0				
71.6	j 9	barren														0	0				
71.2	j 7						3			2						3	2	4			
70.4	j 5						4			2						4	2	4			
70	j 3	2					4				4					6	4	5			
69.8	j7/12	1		1			3		2	2		3		1	1	5	7	4	2	7	
61	J 06/12	1	1	2		1	2		3	4		2				7	9	5		3	
60	J 05/12		2			2	2		4			3	3		1	6	10	5	4	4	
58.8	zu 1		2			2	2		3	2						6	5				
57.2	zu 2		2			3	2		3			2				7	5				
54.2	zu 4		2			2	2		2							6	2				
49.9	zu 7		2			1	3		3					2		6	3				
49.7	zu 9		3			2	2		2			2		2		7	2				
48.5	zu 11		2	2		3	1		3	2			2	2	2	8	7				
45.4	zu 13		2			2	1		2		1					5	3				
44.2	zu 14		3			2	1		2	3						6	5				
42	zu 15	2	12	2	3	1	1		8		1	7	8	4	3	21	24	10	7	5	
34	J 04/12		9						4			3	4			9	11	8	6		
30	J 03/12		5						3							5	3				
28.5	zu 17		6	2	2				2	3			5			10	10	5			
17.5	zu 21b		11	3					7		1			2		14	8				
7.5	zu 24		7	2	2				5	3			3	5	2	11	11				
6.2	zu 25		10						7		1			8		10	8	5	7		
0.1	zu 28	2	6	3					2	2	1			5	2	11	5				